Received: 25 August 2021 | Revised: 22 December 2021 | Accepted: 23 December 2021

DOI: 10.1002/cne.25294

RESEARCH ARTICLE

JCN RESEARCH IN SYSTEMS NEUROSCIENCE THE JOURNAL OF COMPARATIVE NEUROLOGY WILEY

The lateral posterior clock neurons of *Drosophila melanogaster* express three neuropeptides and have multiple connections within the circadian clock network and beyond

Nils Reinhard[1] | Enrico Bertolini[1] | Aika Saito[2] | Manabu Sekiguchi[2] | Taishi Yoshii[2] | Dirk Rieger[1] | Charlotte Helfrich-Förster[1]

[1] Neurobiology and Genetics, Biocenter, University of Würzburg, Würzburg, Germany

[2] Graduate School of Natural Science and Technology, Okayama University, Okayama, Japan

Correspondence
Charlotte Helfrich-Förster, Neurobiology and Genetics, Biocenter, University of Würzburg, Würzburg, Germany.
Email: charlotte.foerster@biozentrum.uni-wuerzburg.de

Present address
Enrico Bertolini, Center for Integrative Genomics, Faculty of Biology and Medicine, University of Lausanne, Lausanne, Switzerland

Funding information
JSPS KAKENHI, Grant/Award Number: 19H03265; Japan Society for the Promotion of Science, Grant/Award Number: 19H03265; Deutsche Forschungsgemeinschaft, Grant/Award Numbers: FO 207/16-1, RI 2411/1-1

Abstract

Drosophila's lateral posterior neurons (LPNs) belong to a small group of circadian clock neurons that is so far not characterized in detail. Thanks to a new highly specific split-Gal4 line, here we describe LPNs' morphology in fine detail, their synaptic connections, daily bimodal expression of neuropeptides, and propose a putative role of this cluster in controlling daily activity and sleep patterns. We found that the three LPNs are heterogeneous. Two of the neurons with similar morphology arborize in the superior medial and lateral protocerebrum and most likely promote sleep. One unique, possibly wakefulness-promoting, neuron with wider arborizations extends from the superior lateral protocerebrum toward the anterior optic tubercle. Both LPN types exhibit manifold connections with the other circadian clock neurons, especially with those that control the flies' morning and evening activity (M- and E-neurons, respectively). In addition, they form synaptic connections with neurons of the mushroom bodies, the fan-shaped body, and with many additional still unidentified neurons. We found that both LPN types rhythmically express three neuropeptides, Allostatin A, Allostatin C, and Diuretic Hormone 31 with maxima in the morning and the evening. The three LPN neuropeptides may, furthermore, signal to the insect hormonal center in the *pars intercerebralis* and contribute to rhythmic modulation of metabolism, feeding, and reproduction. We discuss our findings in the light of anatomical details gained by the recently published hemibrain of a single female fly on the electron microscopic level and of previous functional studies concerning the LPN.

Abbreviations: 5th LN, 5th lateral neuron (formerly called 5th s-LN_v); AME, accessory medulla; AstA, Allatostatin A; $AstA^{SP1}$, AstA positive cells in the SLP (also SLP^{AstA}); AstC, Allatostain C; CA, mushroom body calyx; CRY, Cryptochrome; DD, constant darkness; DenMark, dendritic marker; dFB, dorsal fan-shaped body; DH31, Diuretic hormone 31; DN_{1a}, anterior dorsal neurons 1; DN_{1p}, posterior dorsal neurons 1; DN_2, dorsal neurons 2; DN_3, dorsal neurons 3; E-cells (neurons, peak, activity), evening cells (neurons, peak, activity); EGFP, enhanced green fluorescent protein; E-oscillator, evening oscillator; FB, fan-shaped body of the central complex; Gal4, transcriptional activator from yeast; GFP, green fluorescent protein; Glut, glutamate; HA, hemagglutinin; *hid*, Hid, head involution defective; ITP, Ion transport peptide; LD, light-dark; LH, lateral horn; l-LN_v, large ventrolateral neurons; LN_d, dorsolateral neurons; LO, lobula; LOP, lobula plate; LPN, lateral posterior neurons; MB, mushroom body; M-cells (neurons, peak, activity), morning cells (neurons, peak, activity); MDC, middle dorsal commissure; ME, medulla; nSyb, neuronal Synaptobrevin; PDF, pigment-dispersing factor; PED, mushroom body peduncle; PER, Period; PI, *pars intercerebralis*; PL, *pars lateralis*; PLP, posterior lateral protocerebrum; POC, posterior optic commissure; SCL, superior clamp; s-LNv, small ventrolateral neurons; SLP, superior lateral protocerebrum; SLP^{AstA}, AstA positive cells in the SLP (also $AstA^{SP1}$); SMP, superior medial protocerebrum; sPLPC, superior PLP commissure; *tobi*, *α-Glucosidase target of brain insulin*; UAS, upstream activating sequence

KEYWORDS
activity, circadian clock neurons, insect brain, neuropeptides, sleep, trans-Tango

1 | INTRODUCTION

Endogenous circadian clocks help organisms anticipate the daily 24-h rhythms on earth and timing physiology, metabolism, and behavior to the adequate time of the day. They allow estimating and remembering the time of day and measuring day length in order to predict seasonal changes in the environment. Animals possess a circadian master clock in the brain that modulates their daily behavior and coordinates the clocks in the body. This master clock consists of a network of interacting neurons that are characterized by different morphology, neurochemistry, and physiology and may fulfill different roles in the clock (Herzog et al., 2017; Michel & Meijer, 2020; Mieda, 2020; Rojas et al., 2019; Stengl & Arendt, 2016). The fruit fly, *Drosophila melanogaster*, is an attractive model for studying this clock network in detail because it is composed of only 150 neurons many of which are already largely characterized (reviewed by Beckwith & Ceriani, 2015; Helfrich-Förster, 2017; King & Sehgal, 2020; Top & Young, 2018). These clock neurons are named after their location in the brain and are classically divided into several clusters of lateral and dorsal neurons (Figure 1). As true for other animals, the clock neuron clusters differ in neurochemistry, neurophysiology, and neuroanatomy and play different roles in the circadian system of the flies (Chatterjee et al., 2018; Díaz et al., 2019; Fujiwara et al., 2018; Goda et al., 2018; Guo et al., 2016, 2018; Helfrich-Förster, 2017). The lateral neurons play a dominant role in the clock network and they are the so far best characterized clock neurons, at least those that have their somata in the anterior brain: the small and the large ventrolateral neurons (s-LN_vs and l-LN_vs, respectively), the 5th LN, and the dorsolateral neurons (LN_d; Schubert et al., 2018).

Nevertheless, a further group of lateral neurons with their cell bodies located in the posterior brain is less well known. These cells are called lateral posterior neurons (LPN) and consist of three cells. They have been discovered several years after the other clock neurons because of their weak and temperature-dependent expression of the clock protein Period (Kaneko & Hall, 2000; Kaneko et al., 1997; Miyasako et al., 2007; Shafer et al., 2006; Yoshii et al., 2005). Only recently, their neuronal projections and their putative function in the circadian clock system have been described (Chen et al., 2016; Díaz et al., 2019; Ni et al., 2019). The LPNs express the neuropeptides Allatostatin A (AstA) and Allatostatin C (AstC) and the neurotransmitter glutamate, and they appear to be involved in the control of sleep and feeding (Chen et al., 2016; Ni et al., 2019), in the synchronization of activity to temperature cycles (Miyasako et al., 2007; Yoshii et al., 2005) and in the timing of evening activity under changing environmental conditions (Díaz et al., 2019). The proposed multiple roles of the LPNs require a sophisticated connection to the other clock neurons as well as to neurons downstream of the clock that control these different behaviors. However, the overlap of the LPNs with other neurons that also contain AstA or AstC and the limited availability of Gal4 lines that drive expression specifically in the LPNs has so far prevented

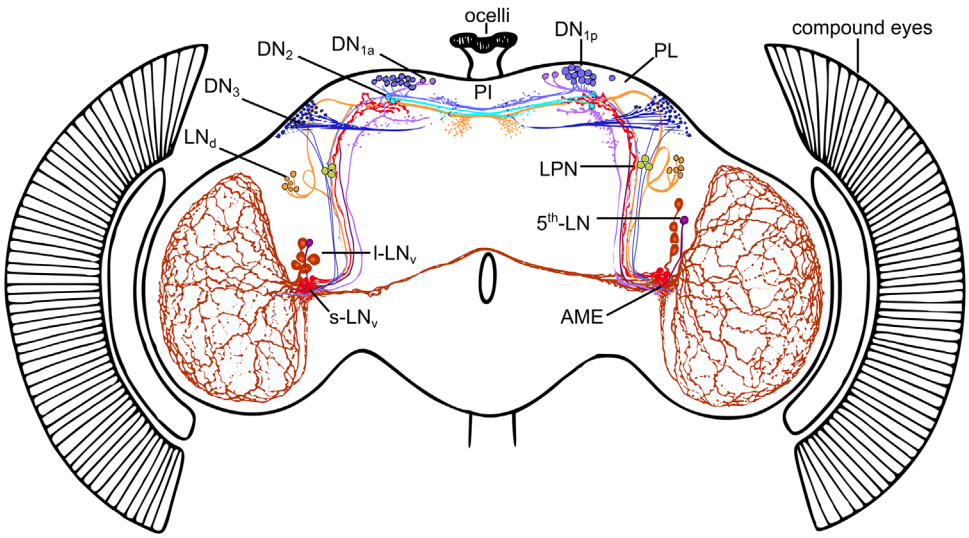

FIGURE 1 The ~150 circadian clock neurons in the brain of *Drosophila melanogaster*. The clock network consists of lateral neurons (s-LN_v, 5th LN, l-LN_v, LN_d, and LPN) and dorsal neurons (DN_{1a}, DN_{1p}, DN_2, and DN_3). Although the somata of the clock neurons are spread in the lateral and dorsal protocerebrum, their neurites are highly connected with each other. Many of them send fibers into the dorsal protocerebrum (including the neurosecretory centers in the *pars intercerebralis* (PI) and pars lateralis (PL)) as well as into the accessory medulla (AME), small neuropils at the base of the medulla. The AME can be regarded as a communication center of the clock neurons. Modified, after Helfrich-Förster et al. (2007) and Schubert et al. (2018). The projections of the lateral posterior neurons (LPNs) are not yet included in this scheme

TABLE 1 Description of the used fly lines

Fly line	Description	Reference
R11B03-p65.AD; R65D05-DBD	*Split-Gal4* line driving in the 3 LPN	(Sekiguchi et al., 2020)
w^{1118}; *R11B03-p65.AD; R65D05-DBD*	*Split-Gal4* line driving in the 3 LPN outcrossed to w^{1118}	
w^{1118}; *UAS-hid;+*	Expressing the apoptosis pathway component Hid under UAS control; outcrossed to w^{1118}	(Zhou et al., 1997)
w; UAS-dTrpA1;+	Expressing the *Drosophila* transient receptor channel dTrpA1 under UAS control for temperature-dependent activation of neurons	(Chen et al., 2016)
w^{1118};+;+	Used for control crossings	Bloomington Cat# 5905
w; +; 10xUAS-myr::GFP	Marking the addressed cells by expression of a membrane-bound myristoylated GFP	(Pfeiffer et al., 2010)
y,w; PBac{20xUAS-6xGFP}VK00018/CyO, P{Wee-P.ph0}BaccWee-P20	Marking the addressed cells by expression of a cytosolic myc-tagged GFP	Bloomington Cat# 52261
UAS-nSyb::EGFP	Marking presynaptic sites (axonal terminals)	(Y. Q. Zhang et al., 2002)
w; UAS-DenMark::mCherry	Marking postsynaptic sites (dendrites)	(Nicolai et al., 2010)
UAS-trans-Tango UAS-myrGFP, QUAS-mtdTomato(3xHA); trans-Tango; +	GFP expression in the Gal4-driver cells and expression of a second reporter (HA or mtdTomato) in possible postsynaptic neurons	(Talay et al., 2017)

a detailed analysis of their fine anatomy and connection with other neurons.

Here, we used a newly generated split-Gal4 transgenic line (Sekiguchi et al., 2020), combined with peptide immunohistochemistry, *trans*-Tango (Talay et al., 2017), and electron microscopic data from the hemibrain (Scheffer et al., 2020) to characterize the anatomy, neurochemistry, and synaptic connections of the LPNs in detail in order to get further insights about their function. We found that the LPNs express a third neuropeptide, the Diuretic hormone 31 (DH31). All three neuropeptides oscillate in a bimodal manner showing peak concentrations around the time of the flies' morning and evening activity. In addition, we reveal so far unknown synaptic connections of the LPNs to other clock neurons that control evening activity, as well as to neuropils that are involved in the control of sleep and arousal. The specific ablation of the LPNs with a cell-death gene significantly reduced morning and evening activity of the flies, which is in consent with the bimodal oscillations of the LPNs' neuropeptide levels. Furthermore, their activation increased sleep during the day and activity during the night indicating that the LPNs play a complex role in the control of the daily sleep–wake cycle.

2 | MATERIALS AND METHODS

2.1 | Fly strains, husbandry, and crossings

Unless stated otherwise, fly strains used in this study were reared on standard cornmeal/agar medium with yeast at 25 ± 0.2°C and 60 ± 5% relative humidity under light-dark cycle (LD) of 12:12 h. All fly lines used are described in Table 1 (including references).

To reveal the anatomy of the LPNs, the *Split-Gal4* line *R11B03-p65.AD; R65D05-DBD* was crossed to a membrane-bound green fluorescent protein (GFP) reporter (10xUAS-myr::GFP) or to a cytoplasmic myc-tagged GFP reporter (20UAS-6xGFP, Table 1). In addition, they were costained with antibodies against the clock protein Period (PER) and different antibodies against neuropeptides to verify their neurochemistry (see immunohistochemical procedure below). To reveal the post- and presynaptic sites of the LPNs, we crossed the *Split-Gal4* line to UAS-DenMark::mCherry and UAS-nSyb::EGFP, respectively (Table 1).

2.2 | Immunocytochemistry

We applied fluorescent immunocytochemistry after the protocol described in Schubert et al. (2018). In brief, flies were fixed as whole animals for 2–3 h in 4% paraformaldehyde after they have been entrained to an LD12:12 cycle for 4–5 days after eclosion. Fixation for anti-PER stainings was performed 1 h before lights-on (ZT23) because PER expression is maximal at this time (Zerr et al., 1990). For neuropeptide immunocytochemistry without PER labeling, fixation was performed around ZT3. Cryptochrome (CRY) immunostaining was performed after exposing flies to three days of constant darkness (DD). After dissecting the brains in phosphate-buffered saline (pH 7.4), they were incubated in blocking solution (5% normal goat serum) overnight and then incubated in the primary antibody solution for ~2 days. Fluorescent labeled secondary antibodies were applied for at least 3 h. All used antibodies are listed in Table 2. The immunostained brains were aligned on a specimen slide with spacers, embedded in Vectashield 1000 mounting medium (Vector Laboratories, Burlingame, CA, USA)

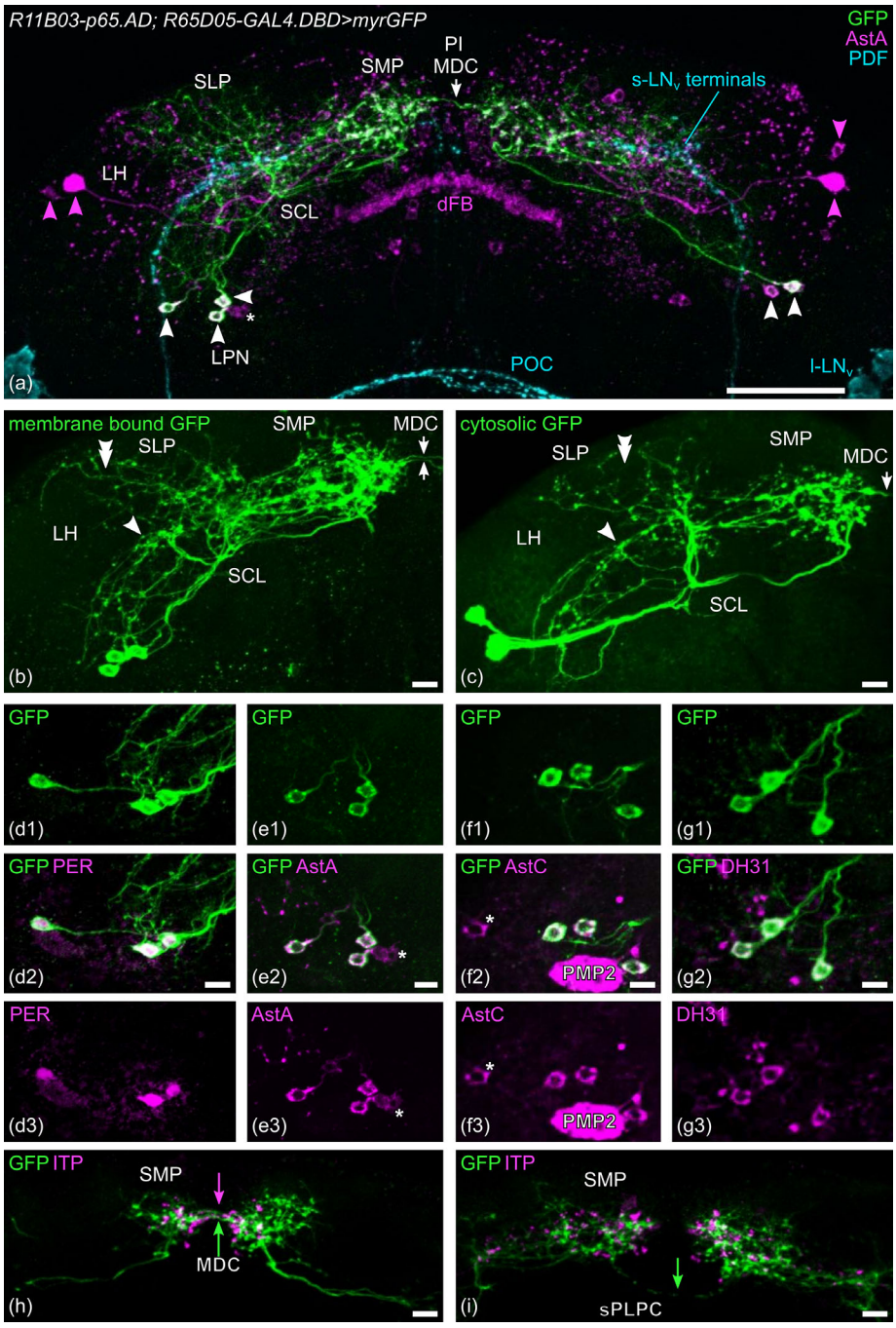

FIGURE 2 The morphology and histochemistry of the lateral posterior neurons (LPNs). (a) Frontal view of the posterior protocerebrum depicting the three LPNs of both brain hemispheres (LPN, white arrowheads) marked with membrane-bound green fluorescent protein (myr-GFP) and anti-Allatostatin A (AstA). AstA is additionally present in the fan-shaped body (FB) of the central complex, in a weakly stained cell body close to the LPNs (*), in a strongly labeled neuron in the superior lateral protocerebrum (SLP), and few weakly stained cell bodies in the same brain region (magenta arrowhead, $AstA^{SP1}$). The LPNs arborize in the superior protocerebrum where they intermingle with the terminals from the small ventrolateral neurons (s-LN_v terminals). They cross the midline of the superior protocerebrum in the middle dorsal commissure (MDC, arrow). The cell bodies of the large ventrolateral neurons (l-LN_vs) are visible at the left and right lower corners of the image. They give rise to fibers in the posterior optic commissure (POC). (b and c) The three LPNs of the left brain hemisphere are marked by membrane-bound (b) and cytosolic (c) GFP, respectively. The arrowheads point to the LPN fibers that overlap with the s-LN_v terminals and the double arrowhead in (c) points to LPN fibers running to the lateral horn (LH). The arrows mark the fibers crossing in the MDC. (d–g) The LPNs are Period (PER)-, Allatostatin A (AstA)-, Allatostatin C (AstC)- and Diuretic hormone 31 (DH31)-positive. The anti-AstC staining shows like the AstA staining an additional weakly stained cell body close to the LPNs (*) as well as the strongly marked PMP2 neurosecretory cell. (h and i) Double-labeling with anti-Ion transport peptide (ITP) shows that the LPN projections to the other brain hemisphere are in close vicinity to the crossing ITP-projections from the 5th LN and the one ITP- and CRY-positive LN_d in the MDC (green and magenta arrow in (h)), but not in the superior posterior lateral protocerebrum commissure (sPLPC) in which only the LPN fibers cross (green arrow in (i))

TABLE 2 Primary and secondary antibodies

Antibody	Directed against	Source	Concentration	Host species	Reference
C7 anti-PDF monoclonal	NSELINSLLSLPKNMNDA-NH_2	DSHB	1:2000	Mouse	(Cyran et al., 2005) RRID: AB_760350
Anti-ITP	GGGDEEEKFNQ	Dircksen	1:4000	Rabbit	(Dircksen et al., 2008) RRID: AB_2315311
Anti-AstA	APSGAQRLYGFGLamide coupled to thyroglobulin	Jena Bioscience GmbH	1:2000	Rabbit	(Vitzthum et al., 1996) RRID: AB_2313972
Anti-AstA	APSGAQRLYGFGL, N-terminal coupled to BSA	Developmental Studies Hybridoma Bank	1:50	Mouse	(Yoon & Stay, 1995) RRID: AB_528076
Anti-AstC	pEVRFRQCYFNPISCF-OH	Veenstra	1:250	Rabbit	(Veenstra et al., 2008) RRID: AB_2753141
Anti-DH31	Full-length peptide	Veenstra	1:500	Rabbit	(D. Park et al., 2008) RRID: AB_2569126
Anti-PER	Full-length protein	Stanewsky	1:2000	Rabbit	(Stanewsky et al., 1997) RRID: AB_2315105
Anti-CRY	His-tagged form of full-length dCRY	Todo	1:2000, preabsorbed on cry^{01} embryos	Rabbit	(Yoshii et al., 2008) RRID: AB_2314242
Anti-GFP	Recombinant full length protein corresponding to GFP	Abcam	1:2000	Chicken	RRID: AB_300798
Anti-mCherry	Full-length protein mCherry	Thermo Scientific	1:2000	Rat	RRID: AB_2536611
Anti-HA	YPYDVPDYA	Roche Diagnostics GmbH	1:100	Rat	(Talay et al., 2017) RRID: AB_2687407
Anti-nc82	Bruchpilot C-terminal aa 1227–1740	Hofbauer	1:50	Mouse	(Wagh et al., 2006) RRID: AB_2314866
AlexaFluor 488 (anti-chicken)	IgY (H+L) chicken	Thermo Scientific	1:200	Goat	RRID: AB_2534096
AlexaFluor 555 (anti-mouse)	IgG (H+L) mouse	Thermo Scientific	1:200	Goat	RRID: AB_141780
AlexaFluor 635 (anti-rabbit)	IgG (H+L) rabbit	Thermo Scientific	1:200	Goat	RRID: AB_2536186
AlexaFluor 647 (anti-mouse)	IgG (H+L) mouse	Thermo Scientific	1:200	Goat	RRID: AB_2535804

and stored at 4°C in darkness until scanning. If not otherwise stated, at least 10 different brains were stained for each antibody or antibody combination.

For the time-course experiment, the flies were entrained to LD 12:12 at 20 ± 0.2°C and collected from ZT0 to ZT21 every 3 h. The entire staining process was done in parallel with the same incubation times for all time points.

2.3 | *trans*-Tango

To reveal putative postsynaptic partners of selected clock neurons, we used *trans*-Tango (Talay et al., 2017). The crosses were reared at 25 ± 0.2°C and the progeny transferred to 18 ± 0.2°C after eclosion for several days, to obtain the accumulation of the postsynaptic signal. In general, we sampled flies after 17, 28, 30, 34, and 53 days at 18°C and found that the postsynaptic signal strength increases significantly with time. Presynaptic neurons were revealed by anti-GFP and postsynaptic neurons by anti-Hemagglutinin (HA) antibody staining (Table 2).

2.4 | Confocal microscopy and image processing

Fluorescence protein expression and antibody staining were visualized and scanned with a Leica SPE confocal microscope (Leica Microsystems, Wetzlar, Germany) equipped with a photomultiplier tube and 488, 532, and 635 nm solid-state lasers for excitation.

We used a 20-fold glycerol immersion objective (HC PL APO; Leica Microsystems) for whole-mount scans and obtained confocal stacks with 2 μm *z*-step size and 1024 × 1024 pixels with a pixel size of 269 × 269 nm. For a more detailed view, we scanned the brains with a resolution of 1024 × 2048 pixels and a z resolution of 1 μm. For the photomultiplier tube, all focal planes were scanned three to four times, and the frames were averaged to reduce background noise. The obtained confocal stacks were maximum projected and analyzed with Fiji (Schindelin et al., 2012). Besides contrast, brightness, and color scheme adjustments, no further manipulations were done to the confocal images, if not stated otherwise. Whenever possible, we

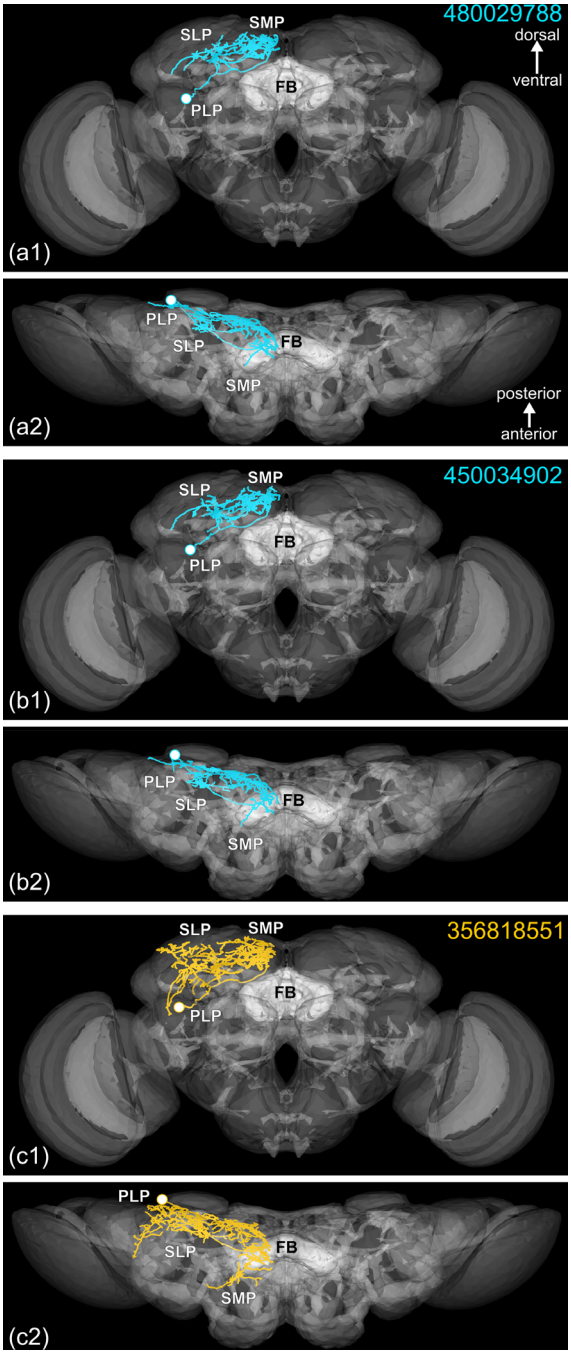

FIGURE 3 The morphology of the lateral posterior neuron (LPN) in the hemibrain. (a) Reconstruction of the as LPN annotated neuron 480029788 with its cell body in the posterior lateral protocerebrum (PLP) and the arborizations in the superior medial protocerebrum (SMP) and superior lateral protocerebrum (SLP). It is missing the fibers in the middle dorsal commissure and the superior posterior lateral protocerebrum commissure. (b) Reconstructions of neuron 450034902 which appears like the neuron from (a). (c) Reconstruction of neuron 356818551 which is similar to the neurons from (a) and (b) besides its broader arborizations in the SMP and SLP which reach further in the anterior superior protocerebrum. Its extended fibers in the SLP follow the fiber tract to the anterior optical tubercle but do not reach it. The frontal view is shown in (x1) and the top view of the reconstructed neurons is shown in (x2). The fan-shaped body (FB) and the brain surface of the standard brain JRC2018F serve as a reference compared our anatomical results with the results gained from the connectome of a single female fly (hemibrain, Scheffer et al., 2020).

2.5 | Quantification of anti-DH31, anti-AstA, and anti-AstC staining intensity

For the quantification of the neuropeptide staining intensities, the freely available software ImageJ (v 1.51r) was used. The confocal images were acquired for all eight time points (ZT0–ZT21) with the same settings as described above (Section 2.4). The anti-GFP signal of the LPNs was used to determine the borders of the cell bodies. For tracing the borders with an octagonal shape, the focal plane with the biggest nucleus diameter was used. In this defined area, the mean pixel intensity of the neuropeptide staining was measured. The mean background intensity was measured three times per hemisphere. For this purpose, squares with an edge length of 15 pixels were used to determine an area near the LPNs. This procedure was done for 20 (DH31) to 22 (AstA/ AstC) hemispheres per time point. Afterward, the background intensity per hemisphere was calculated as an average out of the three background regions. The mean staining intensity of the LPNs was corrected by this value. For better comparison, the staining intensity of the neuropeptides was afterward normalized to the mean staining intensity of each neuropeptide. The time points were tested for significant differences with the Kruskal–Wallis test ($p < .05^{*}$, $p < .01^{**}$, $p < .001^{***}$).

2.6 | Comparison with electron microscopic reconstruction data from the hemibrain

For a comparison of our findings with the reconstructed neurons of the electron microscopic data set from the hemibrain, we used the natverse libraries (v 0.2.4, Bates et al., 2020) for R (v 4.0.5) via RStudio (v 1.3.1093). The neuron-specific information was obtained from the hemibrain data set (Scheffer et al., 2020, v 1.2.1) of the neuprint server (neuprint.janelia.org). The annotation of the neurons was used as a reference, and the identity of the neurons was verified by their morphology and the orientation in the brain. For morphological comparisons, the neurons and brain regions of the hemibrain were transformed into the JRC2018F template space (Bogovic et al., 2020) using xform_brain (nat.templatebrains v 1.0). For the comparison of synaptic sites with the nsyb- and DenMark-stainings, the automatically annotated synapses of the hemibrain and their confidential level were used (Buhmann et al., 2021).

2.7 | Ablation and activation of the LPNs and recording and analysis of rhythms in locomotor activity

Locomotor activity of 3–7 days old male flies was recorded within 1 min bins as described previously (Hermann-Luibl et al., 2014) using

Drosophila Activity Monitors by TriKinetics. The fly tubes positions were fixed by a Plexiglas plate that the infrared beam crossed each fly tube at a distance of ~3 mm from the food. The food consisted of 4% sugar in an aqueous 2% agar gel. Flies were monitored for 10 days in 12 h:12 h light-dark cycles (LD 12:12) with a light intensity of 100 lux at 20 ± 0.2°C and 60% RH ± 0.2% and afterward released in constant darkness (DD). From the recorded days in LD, the days 3–10 were used for activity analysis to make sure the flies were properly entrained. Daily average activity profiles, as well as the standard error, were calculated for each genotype as described in Schlichting and Helfrich-Förster (2015). In short, an average day was calculated for at least 29 flies per genotype and the average day was smoothened with a moving average of 11. For the conditional activation of the LPNs via the TrpA1 channel, the flies were first recorded for 6 days at 20°C ± 0.2°C and 60 RH ± 0.2% (LD 12:12) and afterward recorded for 8 days at 29 ± 0.2°C and 60 RH ± 0.2% (LD 12:12). Recording days 2–6 and 8–14 were used for the analysis to ensure the flies' entrainment. For the days in constant darkness, we performed χ^2 periodogram analyses to determine rhythmicity, free-running period, and rhythm power of the flies using ActogramJ (Schmid et al., 2011).

For temperature entrainment experiments, the flies were first recorded for 3 days under LD 12:12 cycles (100 lux) combined with natural-like temperature cycles (Yoshii et al., 2009). The lowest temperature of 20°C occurred in the morning at ZT0 and then continuously increased until it reached its maximum of 30°C in the early afternoon at ZT8. After 3 days of entrainment, the flies were recorded for 7 days under temperature cycles alone (in DD). Then, the temperature cycle was delayed by 6 h, and the flies' activity was recorded for further 7 consecutive days to test how fast their activity follows the temperature shift.

The number of days, needed for re-entrainment, were determined visually on the actogram for every single fly in a blind test (the actograms were coded and analyzed by one researcher). Flies were judged to be re-entrained when they had reached the same phase relationship of evening activity to the temperature cycle prior to the phase shift. In addition, an entrainment index was calculated for every day based on the method used by Gentile et al. (2013). In brief, the ratio of the flies' activity was calculated between the flies' main evening activity (occurring from ZT9 to ZT12) and the whole activity during daytime (ZT0– ZT12). When the temperature cycle was delayed for 6 h, the time window for the entrainment index calculation was also shifted by 6 h. The entrainment index was normalized to its mean of the first 7 days in DD. Entrainment indices of "1" or higher mean that the flies are entrained to the temperature cycle, while entrainment indices lower than "1" indicate that the flies are not yet re-entrained

Data were analyzed with R (v 4.0.5) using RStudio (v 1.3.1093) with the Rethomics framework (Geissmann et al., 2019) and visualized using the ggplot2 package (v 3.3.3, Wickham, 2016). For the visualization of the actograms, ActogramJ (v 1.0, Schmid et al., 2011) was used and a gaussian kernel with a standard deviation of eight was applied. Activity and sleep data were tested for normal distribution with a Shapiro–Wilk normality test ($p > .05$). If any data set of the comparison was not normally distributed, all data sets of the comparison were handled as not normally distributed. As a nonparametric test, the Mann–Whitney *U* test was used. A *t*-test was used as a parametric test in case of variance homogeneity (Levene's test, $p > .05$); otherwise, a Welch *t*-test was performed. For correction of multiple comparisons, a Bonferroni correction was used.

3 | RESULTS

3.1 | Detailed reconstruction of the LPN arborization patterns

The Split-Gal4 line *R11B03-p65.AD; R65D05-DBD* (Sekiguchi et al., 2020) was very specific for the three LPNs. We did not see any other labeled cells in the central brain, even not when using very strong GFP reporters such as the enhanced membrane-bound and cytosolic GFP we used here (Table 1; Figure 2a–c). Dependent on the strength of the reporter, we observed GFP signal in cells of the optic lobes, which did not project to the central brain. Nevertheless, these cells seemed to be unaffected by other UAS-reporters like UAS-hid. The cytosolic GFP gave stronger staining, while the membrane-bound GFP revealed the fine arborizations of the neurons in greater detail. We confirmed that all three GFP-positive neurons express PER (Figure 2d), AstA (Figure 2e), and AstC (Figure 2f). In addition, we found DH31 as a third neuropeptide (Figure 2g).

The cell bodies of the LPNs were located in the cell body rind of the posterior lateral protocerebrum (PLP). In most cases, we counted exactly three GFP-positive cells. The neurites of the three GFP-positive LPNs fasciculated and ran dorsomedial toward the projections of the LN_vs and DNs in the posterior part of the dorsal brain. In the superior Clamp (SCL), the fiber bundle disentangled into two arms of fibers, one running to the superior lateral protocerebrum (SLP) and the other to the superior medial protocerebrum (SMP). The arm running to the SLP further disentangled and gave rise to multiple fibers. Some overlapped with the pigment-dispersing factor (PDF)-positive terminals from the s-LN_vs (cyan in Figure 2a), others crossed the PDF-positive fibers and extended dorsolaterally to the SLP (double arrowhead in Figure 2c). The fiber arm running to the SMP of the dorsal brain remained fasciculated until it reached the most dorsal part of the SMP laterally of the *pars intercerebralis* (PI, Figure 2a). Here, it split into a fiber network containing pronounced varicosities. The latter overlapped with the fibers from the Ion transport peptide (ITP)-positive LN_d and 5th LN (Figure 2h,i). Two faint connections ran to the contralateral brain hemisphere. The first one consisted of exactly two fibers (e.g., Figure 2b) and crossed in the anterior PI where they run parallel to the ITP-positive fibers in the middle dorsal commissure (MDC, Figure 2h). The second one was fainter and crossed slightly more posterior and ventral through the superior PLP commissure (sPLPC, Figure 2i). We detected the MDC fibers in 82% and the sPLPC fibers in 64% of our specimens (50 stained brains). Due to the fasciculation of all three LPNs, we could not trace the single LPNs, but one of them appeared different from the two others. Its soma was often located apart from the other two cells (see Figure 2c–g), and it appeared to possess a wider arborization

pattern than the others. The reconstructions of the hemibrain support this observation since two of the LPNs showed nearly the same arborization pattern (cyan in Figure 3a,b), while the third LPN showed broader arborizations which extended more anterior in the SMP and SLP (yellow in Figure 3c). In contrast to our observations, no contralateral projection of the LPNs was observed in the hemibrain (Figure 3). Besides the missing commissures, the neurons of the hemibrain, annotated as LPNs (IDs: 356818551, 450034902, 480029788) had the same characteristic arborization pattern in the SLP and SMP as described above and their cell bodies were located in the PLP as typically for the LPNs (Figure 3). With these morphological similarities, we confirm the identity of the three neurons.

3.2 | Evaluation of peptide staining intensity throughout the day

The staining intensity of anti-DH31, anti-AstA, and anti-AstC oscillated in a diurnal manner with one peak around lights-on (ZT 0–3, Figure 4b–e) and a second peak around lights-off (ZT12–15, Figure 4a). Nevertheless, there are distinct staining differences between the three peptides (Figure 4). AstA appeared to cycle with the highest amplitude and had a very high peak in the morning (ZT 0–3, Figure 4b), while the other two peptides showed considerably lower peaks in the morning. For DH31, the staining intensity in the morning and evening was almost of equal height and only a moderate trough was visible in the afternoon (at ZT6–ZT9), while staining was the lowest during the night (at ZT18, Figure 4e). AstC, on the other hand, showed the lowest expression in the afternoon (at ZT 9, Figure 4c) and a less pronounced trough in the night (at ZT18, Figure 4a).

3.3 | Synaptic partners of the LPNs

The LPNs could principally signal to other neurons including the clock neurons in a paracrine fashion via their three neuropeptides (AstA, AstC, and DH31). Indeed, AstC receptors have been found for some LN_ds (Díaz et al., 2019), and DH31 can signal via the PDF receptor on the DN_2s (Goda et al., 2016). In addition, DH31 signals via DH31 receptors on the corazonin-positive neurons in the dorsal brain (Johnson et al., 2005) and AstA and AstC on the corresponding receptors in the insulin-producing cells in the PI (Hentze et al., 2015; C. Zhang et al., 2021).

Since the LPNs express additionally the neurotransmitter glutamate, fast signaling via regular synapses to downstream neurons is also likely (Ni et al., 2019). To reveal the latter, we used the *trans*-Tango system (Talay et al., 2017) and visualized the downstream neurons with anti-HA in flies of different ages (17, 28, 30, 34, and 53 days). The staining differed only in intensity but in all different ages, the same cells could be found.

We found that at least one or both of the two LPNs with their somata located closely together were HA positive (white double arrowheads in Figure 5a,h,i), indicating that these two are interconnected via synapses or that the third LPN signals to them. In addition, in each hemisphere, one to two of the LN_d clock neurons (Figure 5a, e–f) were HA positive. The fibers originating from the HA-positive LN_ds showed the characteristic loop on the surface of the LH on its dorsal way to the posterior side of the brain (horizontal magenta arrowhead in Figure 5a,e,g). Several brains with two labeled LN_ds allowed us to follow the projections of these neurons further. They bifurcated at the dorsal boundary between the LH and the SLP with one branch descending toward the accessory medulla (AME, but not reaching it) and the other main one running to the dorsal part of the brain. From the dorsal part of the brain, the latter branch ran toward the midline of the brain, where it sent varicose terminals to the ipsilateral medial border of the SMP, crossed contralaterally, and did the same on the contralateral border of the SMP (magenta arrowheads in Figure 5a). The arborization pattern of these two LN_ds and counterstaining against CRY (Figure 5f) and ITP (Figure 5g) revealed the HA-positive LN_ds as the CRY-positive but ITP-negative LN_ds (Schubert et al., 2018).

Furthermore, we found HA in several non-clock neurons: one to five conspicuous neurons with a characteristic U-shaped neurite in the posterior protocerebrum (thick magenta arrows in Figure 5a; enlarged pictures in Figure 5b,c) and several neurons with small somata (thin magenta arrows in Figure 5a,b) in the most dorsal superior protocerebrum. All these neurons arborized in the SMP where they formed a dense fiber network that largely overlapped with the fibers coming from the LPNs (magenta arrowheads in Figure 5a) and crossed the midline of the brain in the MDC parallel to the fibers coming from the LPNs (white arrow in Figure 5a). Due to the density of the HA-positive fiber network, we could not separate the projections of single postsynaptic neurons. Nevertheless, we could see that the "U-shaped neurons" projected dorsally and gave birth to two main branches that arborized in the SMP, but did not extend laterally to the LH (Figure 5c,d). The fibers from the small neurons located in the most dorsal SMP projected ventrally but were too faint to be further traced.

We could additionally see HA-labeling in the mushroom bodies (MBs, Figure 5h, j–n) and in one layer of the dorsal fan-shaped body (dFB) of the central complex (Figure 5k). The intensity of the HA signals in the MBs and dFB increased strongly with the age of the flies, while the neurons mentioned above were already strongly stained in the youngest flies. We could trace the neurons that invaded the MBs to several Kenyon cells located in the cell body rind of the calyx (CA, Figure 5h). These cells invaded the CA, the peduncle, and ß and ß' lobes as well as α and α' lobes of the MB (Figure 5h, j–n). In contrast, we were not able to trace the neurons that invaded the fan-shaped body, but according to their arborization pattern in the dFB, they must belong to tangential neurons that have cell bodies in the SLP, axonal arborizations in the 6th layer of the fan-shaped body, and dendrites in the SMP (Donlea et al., 2018; Xie et al., 2019). These dFB neurons have been described by several previous studies due to their prominent role in sleep; they are revealed by the R23E10-Gal4 driver (Donlea et al., 2014, 2018; Ni et al., 2019) and are also called ExFl2 neurons (Xie et al., 2019).

The *trans*-Tango staining was consistent with the presynaptic (output) sites of the LPNs revealed on the ultrastructural level in the

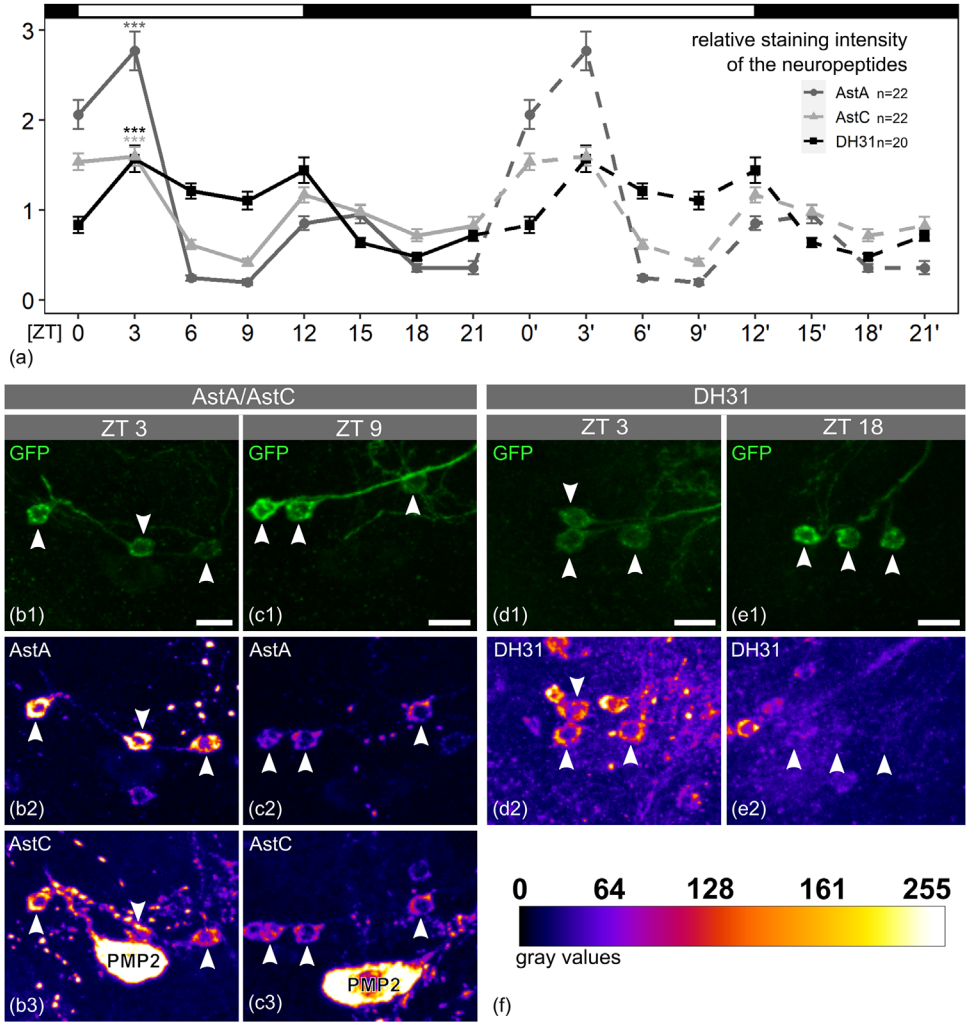

FIGURE 4 Staining intensity of Diuretic hormone 31 (DH31), Allatostatin A (AstA), and Allatostatin C (AstC) (AstC) in the lateral posterior neuron (LPN) throughout the day. (a) Normalized mean staining intensity (±*SEM*) of 20–22 hemispheres of male *D. melanogaster* brains over time (every 3 h) for the neuropeptides Alatostatin A, C (AstA (b2 and c2), AstC (b3 and c3)) and the DH31 (d2 and d3). The staining intensity of the neuropeptides was significantly the highest at ZT3 (Kruskal–Wallis test: $p < .05^{*}$, $p < .01^{**}$, $p < .001^{***}$) and reached the lowest values at ZT9 (for AstA and AstC) or at ZT18 (for DH31). All three neuropeptides showed a bimodal expression pattern. To better reveal the latter, the curves are double-plotted (dashed curves to the right repeat the same data). (b–d) Maximal projections of the *z*-planes containing the cell bodies (white arrowheads) of the LPNs marked by anti-green fluorescent protein (GFP) and antibodies against AstA (b2 and c2), AstC (b3 and c3), and DH31 (d2 and e2) at the highest (ZT3) and the lowest (ZT9/ZT18) staining intensity. Note that close to the LPNs the neurosecretory PMP2 neuron was labeled by anti-AstC. The scale bar represents 10 μm and the staining intensity of the neurons was color-coded according to their gray values (f)

hemibrain (Figure 6a) and by the fluorescent marking of the presynaptic sites via nsyb::GFP (Figure 6b). Most output synapses were found in the SMP and fewer in the SLP, while input synapses (dendrites) were distributed all over the neurites (Figure 6). Again, a similar distribution of input synapses was found on the ultrastructural level (Figure 6a) and with the dendritic marker DenMark (Figure 6c).

Our search for synaptic partners of the LPNs in the hemibrain revealed many postsynaptic and presynaptic neurons with high numbers of synaptic sites (Figure 7a1, b1). While two of the neurons (LPN 480029788 and LPN 450034902) appeared to have a similar number of synapses with the same neurons, the third LPN (LPN 356818551, green) differed in the number of synapses and partners from the other two (Figure 7). The two neurons that were similar in their connections, furthermore, showed strong synaptic contact between each other, while fewer synapses were found between these two and the third LPNs (Figure 7a2, b2). These results nicely supplement our *trans*-Tango stainings.

The LPNs show the highest number of output synapses to neurons of the SMP (up to ~90%), while they get their main input from neurons of the SMP (~60–70%) and SLP (~20–30%, Figure 7c) as well as from the female-specific oviposition inhibitory neurons (oviIN) and a thermosensory neuron of the antennal glomeruli (VP2 + adPN, Figure 7b1). Among the neurons postsynaptic to the LPNs, we found several cells in the hemibrain that had high similarity to the neurons we identified with

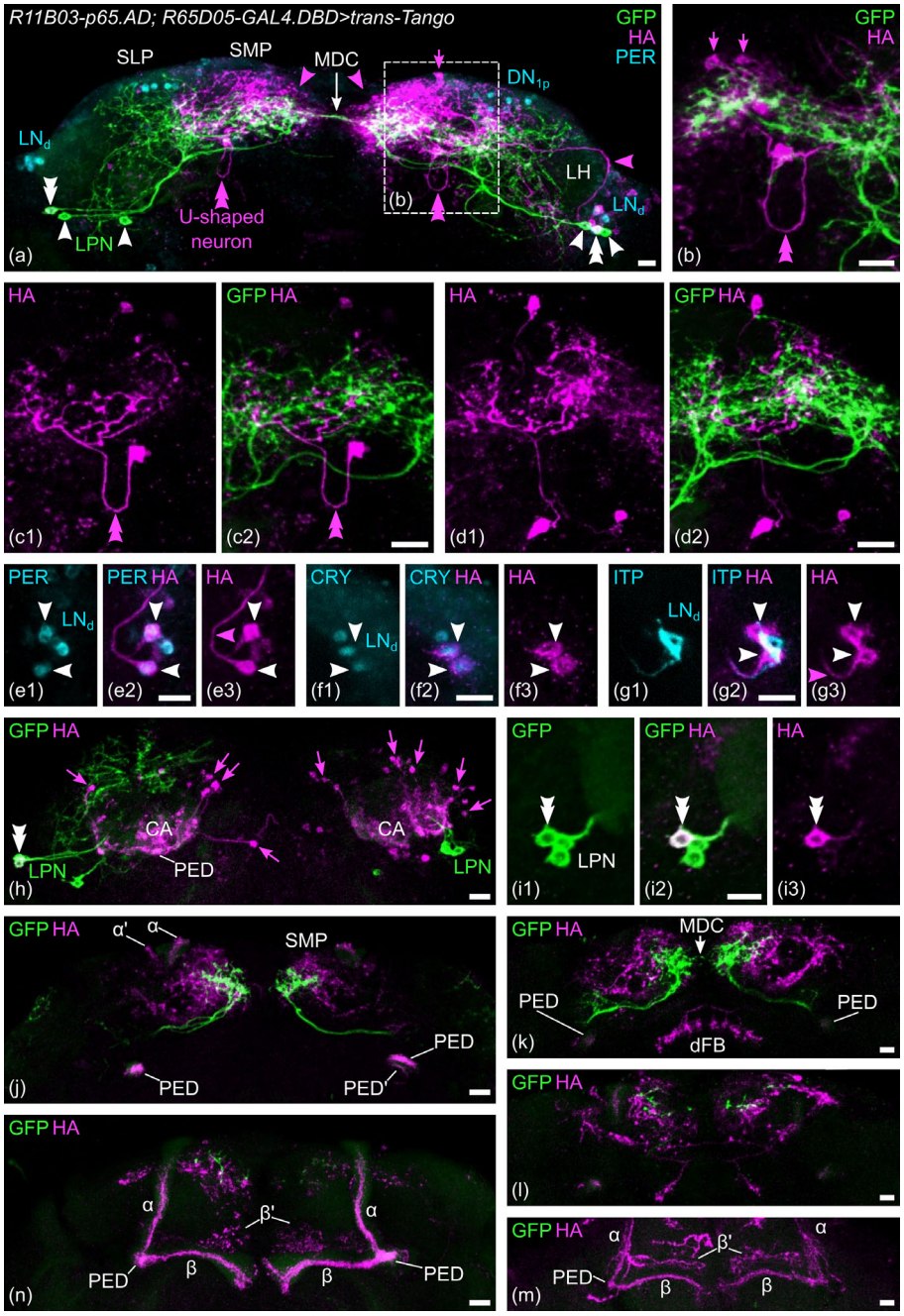

FIGURE 5 Neurons postsynaptic of the lateral posterior neurons (LPNs) revealed by the *trans*-Tango technique. (a) Frontal view of the dorsal protocerebrum with the presynaptic LPNs marked in green (green fluorescent protein, GFP), their postsynaptic partners in magenta (hemagglutinin, HA), and other clock neurons (LN_ds and DN_{1p}s) marked in cyan (labeled with anti-PER). The horizontal magenta arrowhead points to the characteristic loop of the LN_ds, of which two cells were HA positive. The magenta arrows point to the cell body of a small neuron in the superior protocerebrum that projects ventrally (for details see text) and the magenta arrowheads point to the main arborizations stemming from the two LN_ds and the U-shaped neurons, that are postsynaptic of the LPNs. Both the LPNs and the postsynaptic LN_ds cross the midline of the brain via the middle dorsal commissure (MDC, white arrow). The magenta double arrowheads point to the loops of the conspicuous postsynaptic U-shaped neurons that are depicted at higher magnification in (b–d). (b–d) Main arborizations of the U-shaped neurons. They show two main branches, one projecting medially and the other laterally. Both overlap with the posterior arborizations of the LPNs (green, b, c2, and d2), but less so in the anterior superior medial protocerebrum (SMP) parts of the brain to which the LPNs contribute. The magenta arrows in (b) mark two smaller postsynaptic neurons that run ventrally. (e–g) Double labeling of the two postsynaptic LN_ds (magenta, marked by white arrowheads) with anti-PER (e), anti-CRY (f), and anti-ITP (g). (h, j, n) Three consecutive series of 10 confocal stacks from posterior (h) to anterior (n), which depict the postsynaptic mushroom bodies (MB) with calyx (CA). Magenta arrows point to the Kenyon cells that are located dorsally and posteriorly of the calyces (CA). PED, pedunculus; α = alpha lobe; α', alpha prime lobe; β, beta lobe; β',beta prime lobe of the mushroom body. (i) LPNs, of which only one cell is marked by HA (double arrowhead). (k and l) Two consecutive series of five confocal stacks in the middle of the brain, in which the MB and the fan-shaped body (FB) of the central complex are marked by HA. (m) Anterior part of the brain showing labeling of the alpha (α) and beta (β) lobes of the MB by HA

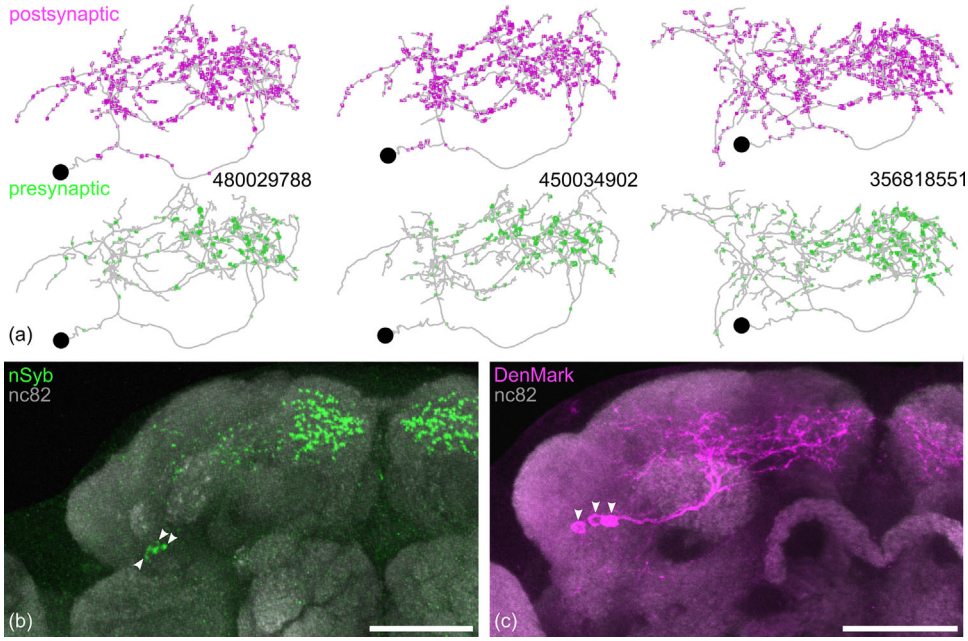

FIGURE 6 Input and output sites of the lateral posterior neuron (LPN). (a) Automatically annotated postsynapses from the hemibrain data set (magenta) as input sites and the presynapses (green) as output sites of the single LPNs. While the input sites are distributed along the whole arborizations of the LPNs the output sites concentrate mainly in the superior medial protocerebrum (SMP). (b) Green fluorescent protein (GFP) tagged nSyb (green) expressed in the axonal endings of the LPNs. Most of the signal was located in the SMP, while only some signal was located in the superior lateral protocerebrum (SLP) which matched with the presynaptic sites from the hemibrain. Maximal projections of the mCherry tagged dendritic marker DenMark (magenta) driven in the LPN are shown in (c). The stainings show the same distribution pattern of the input and output sites as the electron microscopic data of the hemibrain. The scale bars represent 50 μm and the cell bodies of the LPNs are marked by white arrowheads

the *trans*-Tango staining. Among these are the conspicuous "U-shaped neurons" (Figure 7a1, neurons of the groups SMP082-085 marked in orange) and neurons of the dFB that arborize in the 6th layer of the dFB and are called FB6F neurons in the hemibrain (Figure 7a2). While the "U-shaped neurons" possessed numerous synaptic sites with the LPNs (especially with the third LPN that differed from the other two), the FB6F neurons showed fewer synaptic sites with them (but again more frequently with the unique LPN than with the other two).

In contrast to the *trans*-Tango staining, the hemibrain data revealed no trustworthy contacts between the LPNs and other clock neurons as well as no contact to neurons of the mushroom bodies neither as presynaptic nor as postsynaptic partners (Figure 7a2, b2). However, it revealed weak contacts with the DN_{1p}s (eight input synapses from a DN_{1p} type B neuron and a few input/output synapses from/to other DN_{1p}s of the types A and B; Figure 7a2, b2).

3.4 | Effects of LPN manipulation on locomotor activity rhythms and sleep

To test whether the absence of the LPNs affects the locomotor activity pattern of the flies under LD 12:12 conditions, we firstly ablated these neurons by the expression of the apoptotic gene *hid* and secondly activated them by ectopic expression of TrpA1. TrpA1 is a temperature sensor widely used to conditionally activate neurons by increasing the environmental temperature above 24°C (Chen et al., 2016; Hamada et al., 2008; Pulver et al., 2009; Viswanath et al., 2003). By crossing an additional GFP reporter in, we proved with stainings against GFP that the LPNs were indeed ablated by the expression of Hid as an apoptosis pathway component (Figure 8e, arrowheads).

The ablation of the LPNs affected activity levels in the morning and evening of the flies but the overall bimodal activity pattern was unaffected (Figure 8). The LPN-ablated flies still showed anticipatory morning and evening activity and distinct startle responses after lights-on and lights-off, but in comparison to the controls, the anticipatory activity was significantly reduced (Figure 8a, white arrows). The activity levels during the siesta and the night were unaffected. The ablation of the LPNs affected also sleep in a mild but significant manner. The overall sleep amount increased slightly during day and night (Figure 8b, d1). During the day, the increased sleep amount was due to an increase in sleep bout duration (Figure 8d3), while the number of sleep bouts was unchanged (Figure 8d2). During the night, the number of sleep bouts was reduced (Figure 8d2), but sleep bout duration became much longer (Figure 8d3). During the day, the ablation affected mainly the siesta, which became not only deeper but also broader. During the night, the ablation affected sleep predominantly during the second half of the night (Figure 8b).

The activation of the LPNs with TrpA1 yielded complex effects on activity and sleep (Figure 9). As expected after LPN ablation had led to a decrease in morning and evening activity, morning and evening activity

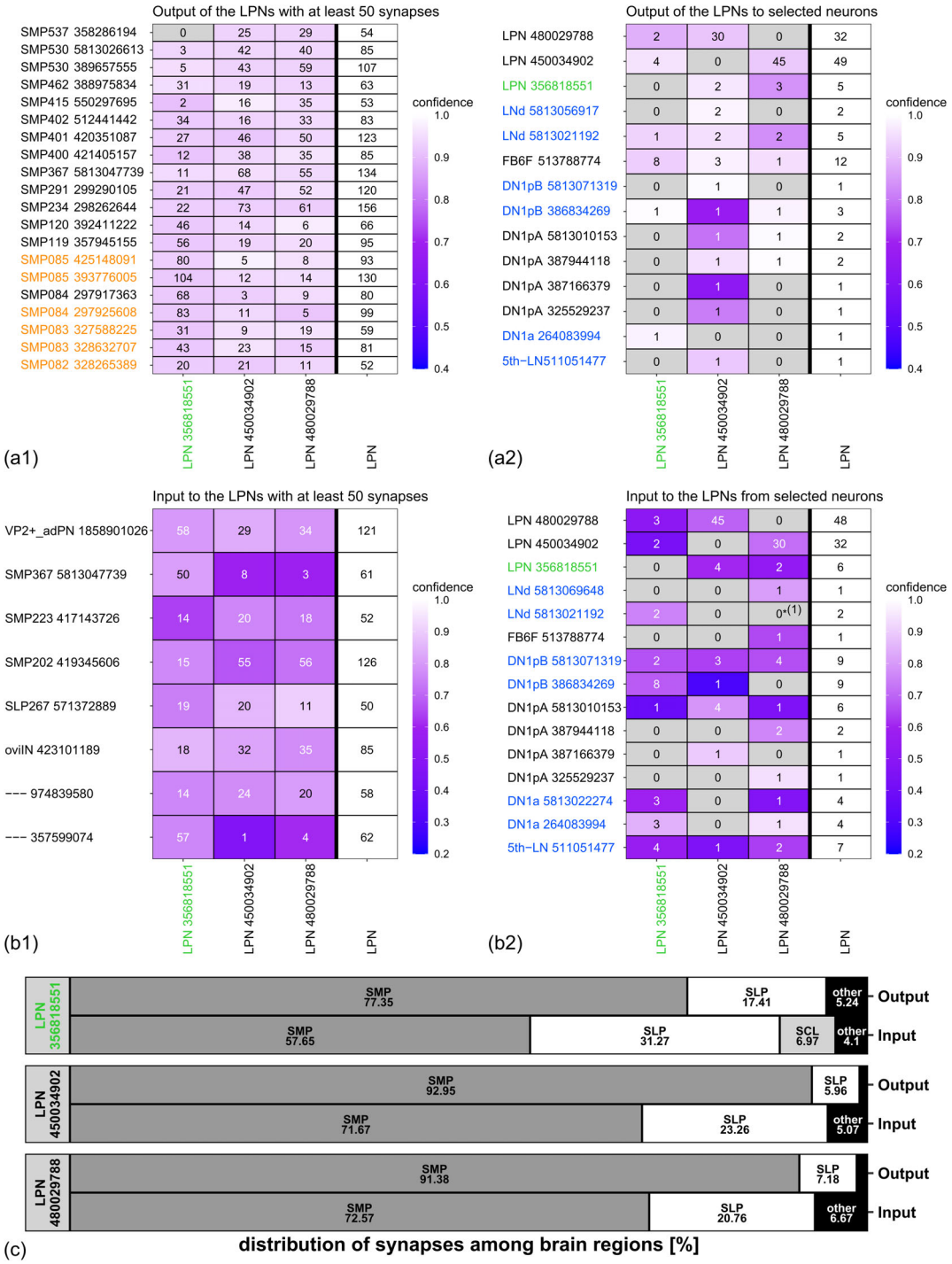

FIGURE 7 Synaptic connections of the lateral posterior neurons (LPNs). (a) Output connectivity of the LPNs to other neurons. (a1) Main output neurons with which the LPNs formed at least 50 synapses. Orange marked neurons depict candidates for the conspicuous "U-shaped" neuron from the *trans*-Tango stainings. (a2) Connectivity to downstream neurons which are members of the clock neurons and the synaptic connections to a neuron of the dorsal fan-shaped body (FB6F) which correlates with our *trans*-Tango findings. CRY-positive neurons are depicted in blue. (b) Input connectivity of the LPNs from other neurons. (b1) Main input neurons of the LPNs which contain temperature sensing neurons from the antennal glomeruli (VP2 + adPN) and an oviposition inhibitory neuron (oviIN 423101189). (b2) Connectivity to upstream neurons which are members of the clock neurons and in addition the FB6F neuron of the dorsal fan-shaped body. While the two morphological similar LPNs (450034902 and480029788) show similar synaptic connections, the unique LPN (green) shows a different connection pattern. CRY-positive neurons are depicted in blue. The color of the tiles represents the mean confidential level of the automatically traced synapses for the corresponding connections. The distribution of the synapses among the brain regions divided into input and output sites is shown in (c). Abbreviations: SCP, superior clamp; SLP, superior lateral protocerebrum; SMP, superior medial protocerebrum. *Correction of the synapsis number after proofreading (only for the LN_ds, automatic annotated synapsis number in brackets)

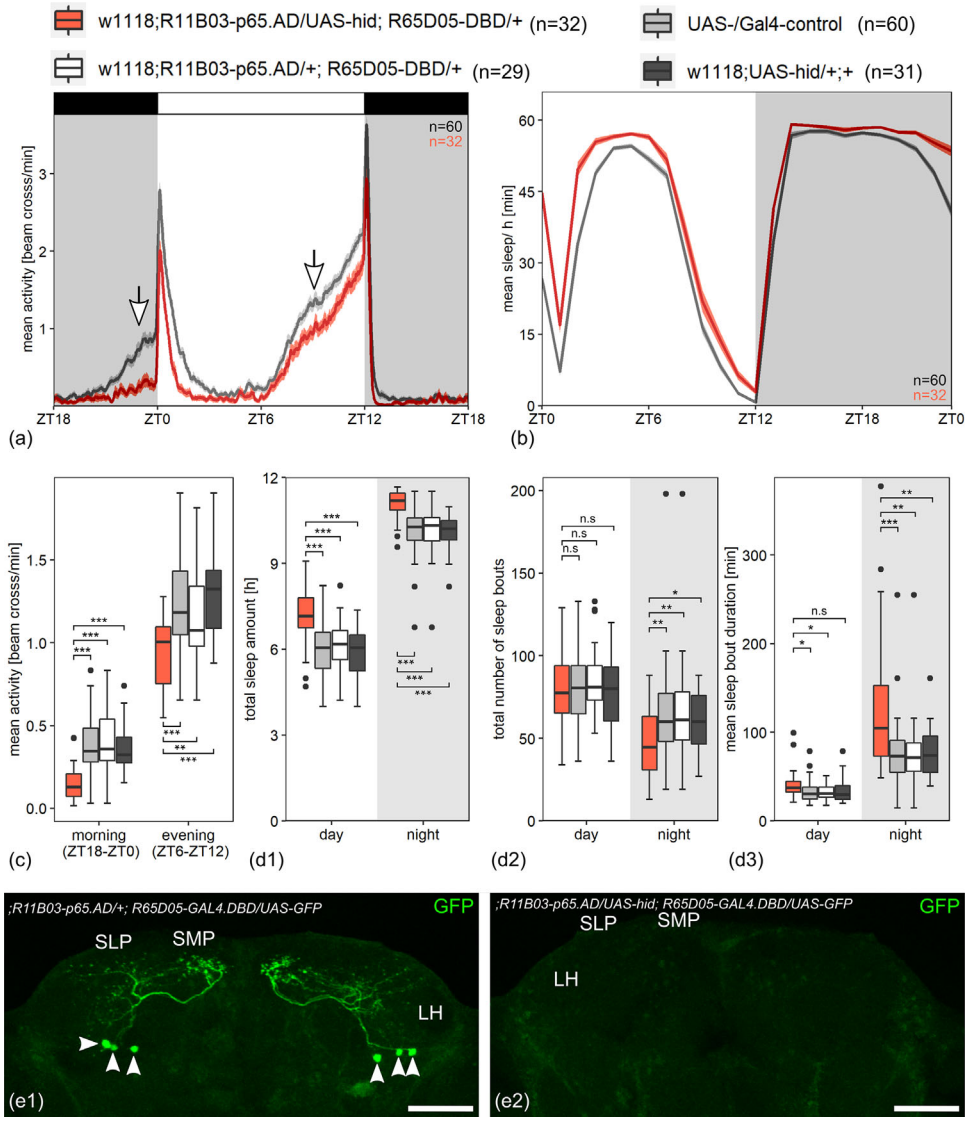

FIGURE 8 Ablation of the lateral posterior neurons (LPNs) reduces morning and evening activity of the flies. (a) Average activity profile ± SE of the experimental line with ablated LPNs (red) and the average day of the pooled controls (gray). While the controls show a strong anticipatory morning and evening activity, the experimental flies show a strongly reduced morning activity as well as a reduced evening activity (arrows). (b) Sleep profile ± SE of the experimental line with ablated LPNs (red) and the pooled controls (gray). The LPN-ablated flies show an increase in sleep over the day and during the night. (c) Mean activity during the morning (ZT18–ZT0) and the evening (ZT6–ZT12) for the experimental line, the UAS (black) and Gal4 controls (white) as well as for the pooled controls (gray). The flies missing the LPNs show significantly lower activity in the morning as well as in the evening compared to the controls. While the activity of the controls in the morning is also different, it is still significantly higher than in the experimental flies; the activity in the evening does not differ between the controls. (d1) Total sleep amount over the day and in the night for the experimental line, the UAS (black) and Gal4 controls (white) as well as for the pooled controls (gray). The experimental flies show a significant increase in sleep compared to the controls independent of the time of the day. (d2) Total number of sleep bouts for the experimental flies and the controls (colors see below). While the number of sleep bouts did not differ during the day, the experimental flies showed a significantly reduced number of sleep bouts in the night. (d3) Mean sleep bout duration during the day and in the night for the experimental flies and the controls (colors see above). After ablation of the LPNs, sleep bout duration increased slightly during the day and strongly during the night ($p < .05$*, $p < .01$**, $p < .001$***). (e1) Immunostaining of the superior protocerebrum with the LPNs marked by green fluorescent protein (GFP) (white arrowheads). (e2) Immunostaining of the superior protocerebrum after ablation of the LPNs via Hid. The scale bar represents 50 μm

significantly increased after TrpA1 channels were activated in the LPNs (Figure 9a,b). In the experimental flies, evening activity was already higher at 20°C as compared to the controls, but at 29°C, it increased strongly in the morning and evening, especially before lights-on and after lights-off (Figure 9a white arrows). In contrast, sleep was slightly lower during the day in the experimental flies than in the controls at 20°C and increased mildly but significantly at 29°C (Figure 9c,d). During the night, sleep was similar in experimental and control flies at 20°C and decreased significantly though again mildly in the experimental flies at 29°C (Figure 9c,d). While the observed increase of sleep

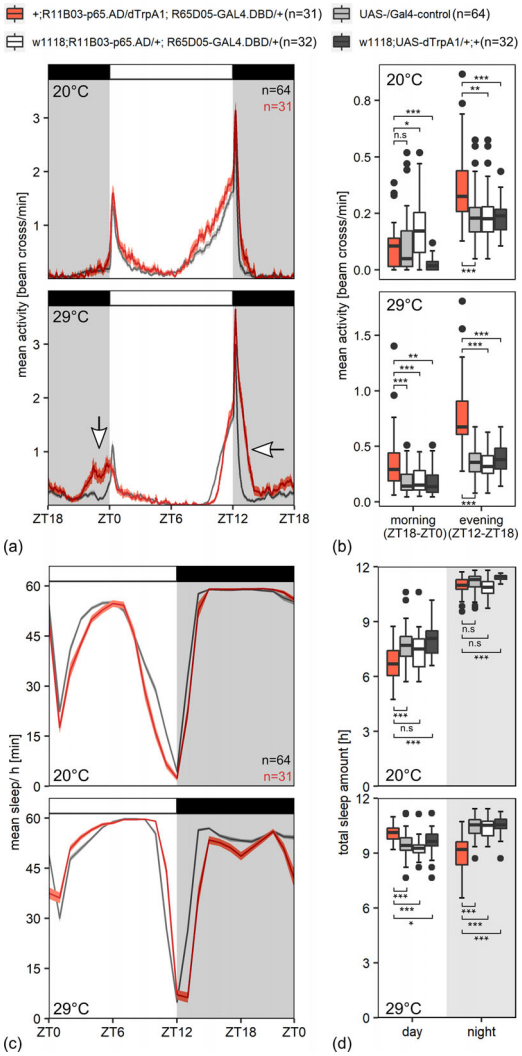

FIGURE 9 Conditional activation of the lateral posterior neurons (LPNs) has complex effects on activity and sleep. (a) Average activity profile ± SE of the experimental line with dTrpA1 expressing LPNs (red) and of the pooled controls (gray) at 20°C. At 20°C both control flies and experimental flies show a normal bimodal activity pattern with morning and evening activity with a slightly higher activity level of the experimental flies in the second half of the day. After conditional activation of the LPNs, the experimental flies show a strong increase in morning activity before lights-on as well as a deeper and broader siesta and an increased evening activity after lights-off (arrows). (b) Mean activity of the flies during the morning (ZT18-ZT0) and the evening (ZT12-ZT18). The experimental flies showed a slightly higher evening activity than the controls at 20°C, while morning activity was similar. After conditional activation of the LPNs at 29°C, the experimental flies reduced evening activity before lights-off and significantly increased evening activity after lights-off as well as morning activity before lights-on. (c) Sleep profile ± SE of the experimental line with dTrpA1 expressing LPNs (red) and the pooled controls (gray) at 20 and 29°C. At 20°C, no significant difference toward both controls could be found, while after conditional activation of the LPNs (29°C), the experimental flies showed an increase in sleep over the day and a reduced sleep in the night. (d) Total sleep amount of the flies at 20 and 29°C divided by day and night time. While the flies' sleep significantly increased during the day after activating the LPNs, the flies slept significantly less during the night during the day after LPN activation is principally in line with previous results obtained by Chen et al. (2016) after TrpA1 activation in the LPNs, the observed decrease in the night does not fit at all. Furthermore, the effects on sleep, we report here, are generally much milder than those found by Chen et al. (2016). Chen et al. (2016) used two different AstA-Gal4 lines to activate the LPNs (the LPNs were called PLP neurons in this study). Importantly, we could reproduce the results of Chen et al. (2016), using these AstA-Gal4 lines (Reinhard, unpublished).

To test the importance of the LPNs for maintaining free-running rhythms under constant conditions, we monitored flies with ablated LPNs (see above) plus the relevant controls under DD conditions. All flies maintained robust rhythmicity with similar periods, indicating that the LPNs are not necessary for controlling circadian rhythmicity (Table 3). Nevertheless, the rhythm power of the LPN ablated flies was significantly lower than in the control strains, suggesting that the LPNs contribute to the robustness of circadian rhythmicity.

To test the importance of the LPNs for temperature entrainment, we monitored the activity of flies with ablated LPNs under phase-shifted natural-like temperature cycles in DD (Figure 10). We found that the flies lacking the LPNs were still capable of entraining to temperature cycles, but their activity appeared less consolidated than that of the controls. For example, during entrainment to temperature cycles alone, their activity was significantly reduced during the evening bout (Figure 10b) and appeared more distributed over the entire day (Figure 10a). In addition, the flies with ablated LPNs took significantly longer to re-entrain to the phase-shifted temperature cycles as judged from visual inspection of the actograms (Figure 10c) and their entrainment indices (Figure 10d). Together, these results indicate that the LPNs contribute to the flies' temperature entrainment.

4 | DISCUSSION

Here, we characterize the morphology and neuropeptide expression of *Drosophila*'s LPN in more detail than done before. Overall, we confirm previous descriptions and add important details that reveal a so far unknown degree of heterogeneity within this small population of clock cells. Additionally, we describe synaptic connections of the LPNs with many areas and neurons in the brain, including connections with other neurons of the clock network. In the following, we will discuss our findings in the light of previous results, especially with the anatomical details gained by the recently published hemibrain connectome of a single female fly on the electron microscopic level and of numerous functional studies that attributed specific roles to the clock neuron groups. Eventually, we provide evidence that the LPNs have a crucial role in modulating the morning and evening activity of fruit flies and propose a network model (Figure 11). In addition, the LPNs contribute to temperature entrainment but are not important for controlling rhythmicity under DD conditions.

TABLE 3 Period length and power of the lateral posterior neuron (LPN)-ablated flies and the controls under constant darkness (DD) conditions

	w^{1118};R11B03-AD/UAS-hid;R65D05-DBD/+ ($n = 23$)	w^{1118};R11B03-AD/+;R65D05-DBD/+ ($n = 30$)	w^{1118};UAS-hid/+;+ ($n = 32$)
Period length (h)	23.65 ± 0.07 (n.s/n.s)	23.67 ± 0.05	23.60 ± 0.05
Power	117.26 ± 7.33 (***/***)	230.21 ± 14.15	178.88 ± 10.09
Rhythmicity (%)	90.63	100	95.65

Abbreviation: n.s, not significant. $P < 0.001$ ***, significant levels compared to the Gal4- and UAS-control.

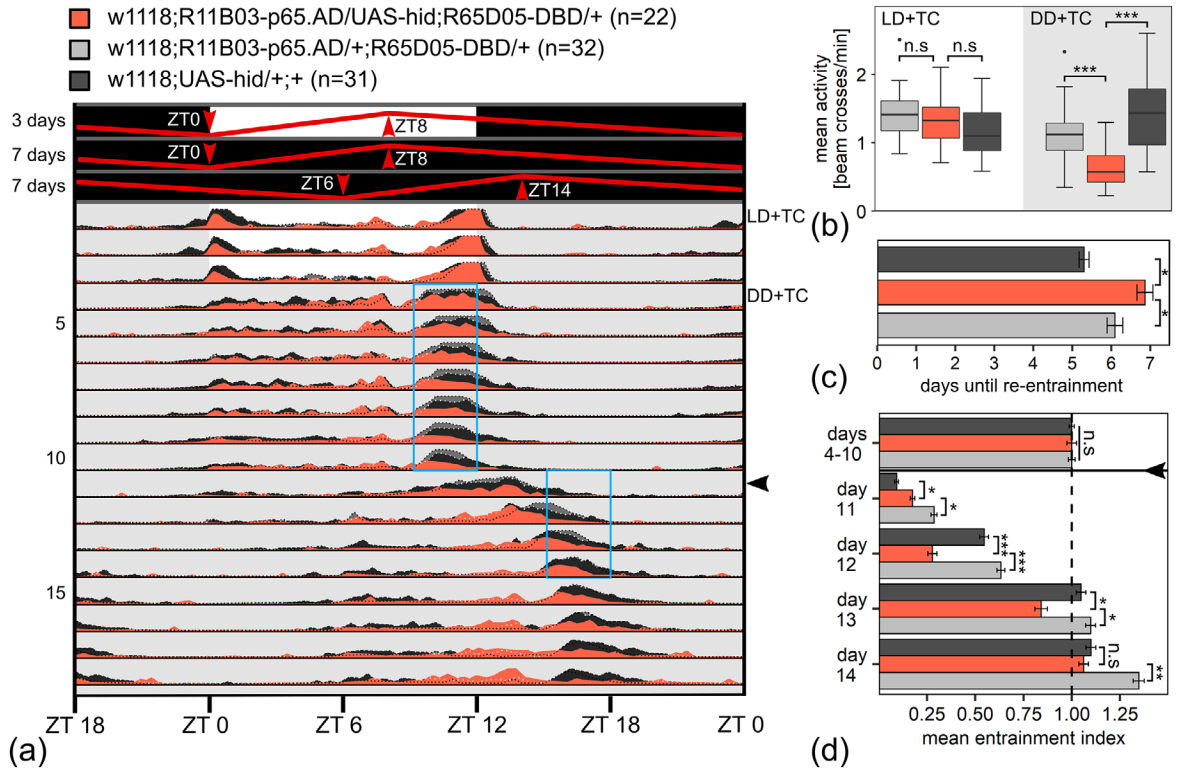

FIGURE 10 Ablation of the lateral posterior neurons (LPNs) slightly impairs temperature entrainment under constant dark conditions (DD). (a) Average actogram showing the activity of control flies (in light and dark gray) and flies with ablated LPNs (in red) during an experiment with a phase-shifted temperature cycle. During the first 3 days, the flies were recorded at a combination of light-dark (LD) and natural-like temperature (TC) cycles. As indicated in the bars on top of the actogram, the temperature was minimal at lights-on (ZT0) and then steadily increased until it reached its maximum in the early afternoon (ZT8) and then decreased again. On day 4, the lights remained switched off, and the flies were recorded under the temperature cycle in constant darkness (DD + TC). On day 11, the temperature cycle was delayed by 6 h (horizontal arrowhead). The number of recorded flies per genotype is indicated on top. (b) Mean activity of the three genotypes during the evening bout of activity (ZT9–ZT12) under the combination of light-dark and temperature cycles (LD + TC) and during temperature cycles alone (DD + TC). For the calculation of the mean activity, the last 3 days of LD + TC and DD + TC (before the shift) were used. (c) Mean number of days (±*SEM*) that the three genotypes needed to re-entrain to temperature cycles after the 6 h delay. (d) Entrainment indices calculated before and several days after the 6 h delay of the temperature cycle. The time of the shift is indicated by a horizontal arrowhead. The blue boxes in the average actogram mark the evening activity of the flies during the temperature cycles before and after the shift. The indicated intervals were used to calculate the shown entrainment indices. Significant differences between controls and flies with ablated LPNs are marked by asterisks ($p < .05$*, $p < .01$**, $p < .001$***; n.s., not significant)

4.1 | The LPNs' arborization pattern and connections with other neurons

Our results gained by analyzing the expression of a novel Split-Gal4 line (Sekiguchi et al., 2020) largely match the projection pattern of the three LPNs from the hemibrain (Scheffer et al., 2020) with one exception. We found projections of at least one LPN to the other brain hemisphere (in the MDC and sPLPC) that were overlooked in the hemibrain, most probably because it lacks some morphological details related to commissures. Nevertheless, the hemibrain is superb

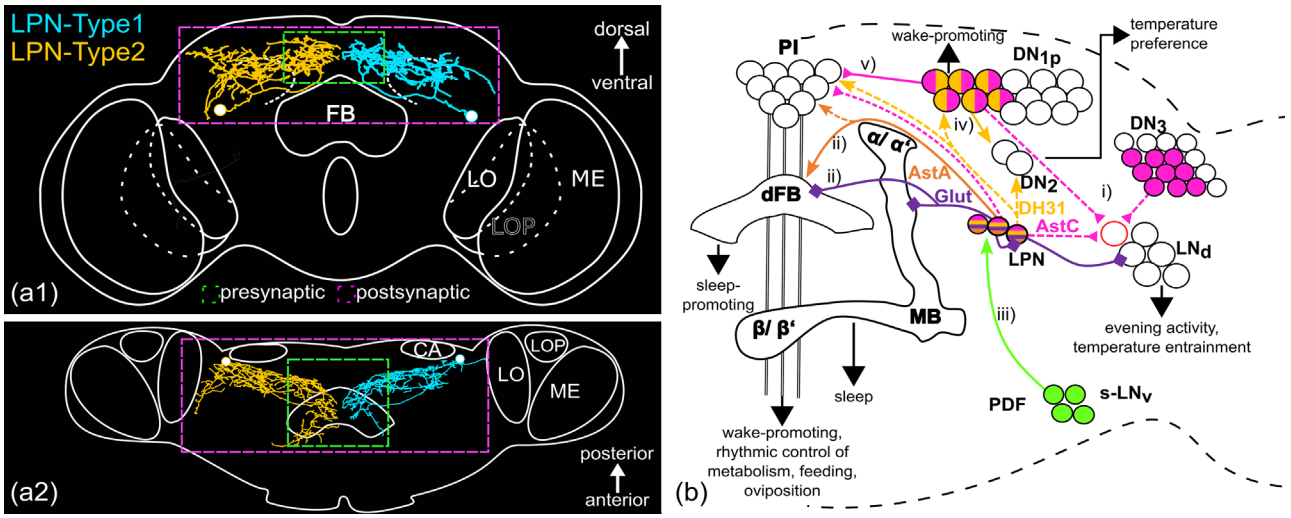

FIGURE 11 Schematic model of the lateral posterior neurons' (LPNs) role in the clock network of *D. melanogaster*. (a) Schematic overview of the two LPN types with their arborizations in the superior medial protocerebrum (SMP) and superior lateral protocerebrum (SLP) and their main input (magenta) and output (green) regions. While the main output region is restricted to the SMP, the input sites are distributed over the whole arborizations in the SMP and SLP. (a1) Frontal view and (a2) Top view. (b) Hypothetical role of the LPNs in the clock network dependent on the different neuropeptides and neurotransmitters. The LPNs get input from the s-LN_vs via pigment-dispersing factor (PDF) (iii, Chen et al., 2016) which most likely controls the cycling of the neuropeptides in the LPNs. The three neurons form synaptic contact with two CRY-positive but ITP-negative LN_ds. In addition, they most likely signal via Allatostatin C (AstC) to at least one LN_d (i, Diaz et al., 2019). Via this pathway, they might modulate the evening activity and might mediate temperature entrainment of the flies together with AstC signaling from the DN_{1p}s and DN_3s (i, Diaz et al., 2019). The LPNs have also synaptic contact to the dorsal fan-shaped body (dFB), which supports the results from Ni et al. (2019) and Chen et al. (2016) who showed the involvement of the LPNs in sleep regulation (ii). In addition, the LPN could regulate sleep via glutamate signaling to the mushroom bodies (MB). Via Allatostatin A (AstA), the LPNs could furthermore signal to the *pars intercerebralis* (PI) leading to a rhythmic modulation of feeding and metabolism (Chen et al., 2016). The LPN could also affect temperature preference directly by signaling via DH31 to the DN_2s or indirectly by signaling to the DN_{1p}s that then signal via DH31 to the DN_2s (iv, Goda et al., 2016). Furthermore, DH31 signaling to the $DN1_p$s and the PI might cause a wake-promoting function of the LPNs. Next to DH31, the LPNs might also signal via AstC to the PI and influence via this pathway rhythmic oviposition like it was already shown for the $DN1_p$s (v, C. Zhang et al., 2021). Abbreviations: LO, lobula; LOP, lobula plate; ME, medulla, CA, calyx

in characterizing single neurons of a cluster. Our confocal-microscopic studies could not unequivocally distinguish individual neurons of the LPNs because their neurites largely fasciculated with each other, but we observed that one LPN differed in the position of the cell body and had most likely a different morphology than the other two. The three-dimensional reconstructions of the hemibrain confirmed our hypothesis in this regard. One LPN showed a much broader arborization pattern in the SMP and SLP than the other two, which looked very similar. The difference between the LPNs is also supported by the analysis of their synaptic connections to other neurons or with themselves (judged from the automatically annotated synapses in the hemibrain; Scheffer et al., 2020). While the two similar LPNs seem to be in strong synaptic contact with each other, as also shown in our *trans*-Tango data, the third LPN has only a few contacts with the other two LPNs. The unique LPN instead showed much more output synapses to the "U-shaped" SMP neurons than the other two LPNs that appeared to signal to many other still uncharacterized neurons in the SMP. In addition, the unique LPN received more input from neurons in the SLP and especially the superior clamp than the other two LPNs. The superior clamp is connected with the SLP and the anterior optic tubercles (Yu et al., 2013), which fits the anterior projections of the unique LPN.

4.1.1 | Connections between the LPNs and other clock neurons

Our *trans*-Tango staining revealed the two CRY-positive but ITP-negative LN_ds as postsynaptic partners of the LPNs. The HA signal in these two LN_ds was already visible in 17 days young flies, meaning that it accumulated faster than in most of the other postsynaptic cells (Talay et al., 2017), which were all nonclock neurons. This speaks for strong synaptic contacts between the LPNs and LN_ds that should be visible on the electron microscopical level. However, the hemibrain revealed only a few synapses between the LPNs and the LN_ds (Scheffer et al., 2020). Since the CRY-positive LN_ds project contralaterally (Schubert et al., 2018), it is possible that the LPNs signal to them from the contralateral brain hemispheres, which is absent in the hemibrain. At present, it is not clear which LPN has the strongest connections to the CRY-positive LN_ds, but when taking the confidential level of the automatic traced

single synapses into account (Buhmann et al., 2021), we can say that all three LPNs signal to at least one CRY-positive LN_d which is also covered by our *trans*-Tango experiments. The hemibrain revealed also synapses between the LPNs and other clock neurons that we missed in our *trans*-Tango experiments. For example, it suggests input and output synapses between the LPNs and certain DNs as well as between the LPNs and the 5th LN. These results indicate that the synaptic connections of the LPNs within the clock network are numerous. In addition, they appear highly complex because there seem to exist differences between the unique LPN and the other two LPNs as well as between the two similar LPNs. Future investigations are necessary to confirm all these putative connections.

4.1.2 | Synaptic connections between the LPNs and neurons that are putatively downstream of the circadian clock

Our *trans*-Tango stainings revealed strong HA signals in unknown conspicuous neurons, which we called "U-shaped" neurons as well as weaker signals that accumulated with the age of the flies in the dFB and MBs. In the hemibrain, we could identify similar "U-shaped" neurons (from the neuron groups SMP084-085) and dFB neurons (called FB6F neurons) that were postsynaptic to the LPNs, while the MBs were not among the postsynaptic partners of the LPNs in the hemibrain. The hemibrain revealed many synapses between the LPNs and the "U-shaped" neurons, which fits the strong HA staining already in young flies in our *trans*-Tango experiments. In contrast, the synaptic connections between the LPNs and the FB6F neurons were sparse in the hemibrain, which fits again to our *trans*-Tango staining: HA accumulated slowly in the FB6F neurons and was strongly visible in old flies. The FB6F neurons are most likely identical with the ExFl2 neurons (Xie et al., 2019) that are also revealed by R23E10-Gal4, which includes an enhancer from the AstA receptor (Donlea et al., 2014, 2018; Ni et al., 2019; Pimentel et al., 2016). These neurons are tangential FB neurons arborizing in the 6th layer of the dFB and strongly sleep-promoting (see below).

We could not explain for sure, why no synapses between the LPNs and MBs have been detected in the hemibrain, but obviously, the number of such synapses is very low since *trans*-Tango revealed these only after HA accumulated for many days. These synapses may have simply not been detected in the one female fly used for the hemibrain. It is also possible that the LPNs change their synaptic connectivity over the time of day as do other clock neurons (Duhart et al., 2020). By chance, the single fly may have been fixed at a time at which no synapses between the LPNs and the MBs were formed. More EM samples at different times of the day may be necessary to solve this issue. In the present study, we stained >10 brains of male flies, additionally, *trans*-Tango has the advantage of being independent of daily variations and can detect even weaker synaptic connections if HA could accumulate for several days. Therefore, we assume that the connections we found between the LPNs and the MBs are real.

4.2 | Putative functional relevance of the LPN synaptic connections

While we have no information about the function of the "U-shaped" neurons, the synaptic connections between the LPNs and the clock neurons as well as between the LPNs and dFB and MB neurons support LPN functions that were assessed in former studies and that will be discussed in the following.

The first LPN studies have implicated them in the synchronization of activity to temperature cycles (Miyasako et al., 2007; Yoshii et al., 2005), while later studies showed that they are dispensable for normal temperature entrainment under constant light conditions (Gentile et al., 2013) and do not change their neuronal activity after temperature changes (Yadlapalli et al., 2018). Here, we show that LPN-ablated flies take longer to re-entrain to a delay of the temperature cycle under DD conditions than control flies, indicating that the LPNs contribute temperature entrainment, even though temperature entrainment does not depend on them.

Furthermore, recent studies have suggested a role of the LPNs in the timing of evening activity under changing environmental conditions (Díaz et al., 2019). Both roles can be explained by synaptic LPN-signaling to the LN_ds in addition to their already shown neuropeptidergic signaling (Díaz et al., 2019). The CRY-positive LN_ds belong to the Evening (E) neurons that control the flies' evening activity (reviewed by Yoshii et al., 2012). Timing of evening activity is highly flexible and quickly adapts to environmental fluctuations such as changes in temperature and illumination (Díaz et al., 2019; Dubruille & Emery, 2008; Majercak et al., 1999; Rieger et al., 2003, 2007; Schlichting et al., 2019). According to the hemibrain (Scheffer et al., 2020), the LPNs receive input from a thermosensory neuron of the antennal glomeruli (VP2 + adPN; Figure 7b1). Together with our behavioral results, this makes it very likely that they are involved in temperature sensing, in addition to the probably more important DN_{1p}s that even respond with neuronal activity to temperature changes (Yadlapalli et al., 2018). So far, no synaptic connections from the temperature sensing DN_{1p}s neurons to the evening activity controlling LN_ds have been shown. Here, we demonstrate for the first time synaptic connections between the LPNs and at least one of the CRY-positive but ITP-negative LN_ds. In addition, the hemibrain revealed that several DN_{1p}s might signal to at least one of the LPNs. Thus, the timing of E activity may be modulated in a temperature-dependent manner via glutamate either directly from the LPNs or indirectly from the DN_{1p}s via the LPNs. Most interestingly, the synaptic connections between the LPNs and the E neurons appear bilateral and even the 5th LN, which also belongs to the E neurons (Rieger et al., 2006) might synapse on the LPNs. In summary, the LPNs appear tightly interlinked with the E neurons and as we will see below (Section 4.3) that this is not only true regarding synapses but also concerning modulatory neuropeptides.

Our *trans*-Tango data also provide the anatomical basis for another suggested LPN role—their sleep-promoting effects (Chen et al., 2016; Guo et al., 2018; Ni et al., 2019). The MBs and the central complex have been shown to be involved in sleep (Donlea et al., 2014, 2018;

Joiner et al., 2006; Liu et al., 2016; Pitman et al., 2006; reviewed by Helfrich-Förster, 2018). Especially layer 6 of the dFB, which shows prominent *trans*-Tango staining in our study, is well known for getting signals from sleep-promoting neurons (Donlea et al., 2014, 2018). The LPNs are such neurons. Ni et al. (2019) showed that the LPNs together with an additional $AstA^{SP1}$ neuron (named "SLP^{AstA}" neuron by Donlea et al., 2018) signal via glutaminergic excitatory synaptic connections to the dFB and increase sleep bout length in the night. Our *trans*-Tango stainings confirm the proposed synaptic signaling of the LPNs to neurons in the dFB. In addition, we found synaptic signaling between the LPNs and α-/β- plus α'-/β'-Kenyon cells, which invade regions of the MB that are well known to be involved in the sleep network (Joiner et al., 2006; Pitman et al., 2006). Altogether, our results support the suggested role of the LPNs in the regulation of sleep (see also Section 4.3).

4.3 | Cyclic expression of neuropeptides in the LPNs

Already early studies have shown that animal clock neurons are rich in neuropeptides that often colocalize in the same neurons and fulfill multiple modulatory functions in the circadian system (reviewed in Helfrich-Förster, 2014). The LPNs express three neuropeptides at once: AstA (Chen et al., 2016), AstC (Díaz et al., 2019), and as found here also DH31. All three peptides are expressed rhythmically and can therefore modulate all those neurons in a paracrine rhythmic fashion, which are in the vicinity of the LPNs and possess the relevant neuropeptide receptors,

In *Drosophila*, the PDF is the so far best-characterized neuropeptide in the circadian clock. PDF is expressed rhythmically with a pronounced peak in the morning (J. H. Park et al., 2000). The perhaps most important role of PDF lies in the communication between different clock neurons (Helfrich-Förster, 2014; Klose et al., 2016; Liang et al., 2016). Although PDF is only present in eight of the ~75 clock neurons per hemisphere (in the s-LN_vs and the l-LN_vs, Helfrich-Förster, 1995), about half of the clock neurons express the PDF receptor (Im & Taghert, 2010). The LPNs are among the PDF-receptor expressing neurons and are activated by PDF signaling from the s-LN_vs (Chen et al., 2016). This activation happens most likely in the morning when PDF is released from the s-LN_vs terminals that largely overlap with the arborizations of the LPNs in the SLP (Figure 2a). Thus, the LPNs are not only synaptically connected with the E neurons but via neuropeptide signaling also with the M neurons as shown by Chen et al. (2016). The PDF peak in the s-LN_vs nicely coincides with the M peak of the bimodal expressed neuropeptides AstA, AstC, and DH31 of the LPNs, suggesting that this M peak depends on PDF signaling, while their E peak may depend on signaling from the E cells (LN_ds and 5th LN; see Section 4.2).

Especially AstA shows a prominent peak in the morning and a second less pronounced one in the evening. AstA is strongly sleep-promoting (Chen et al., 2016; Donlea et al., 2018; Ni et al., 2019) and acts together with glutamate on the dFB (Donlea et al., 2018; Ni et al., 2019). While glutamate is needed for consolidated sleep in the night (Ni et al., 2019), AstA signaling to the dFB appeared especially sleep-promoting during the day and to a lesser degree in the night (Donlea et al., 2018; Ni et al., 2019). This fits perfectly with the AstA expression profile in the LPNs. Nevertheless, AstA is not only sleep-promoting but is additionally also involved in metabolism and feeding (Chen et al., 2016; Hentze et al., 2015; Hergarden et al., 2012). Part of these effects are mediated by insulin-like peptide expressing neurosecretory cells in the PI, which are activated by AstA via the AstA receptor Dar-2 (Hentze et al., 2015). The LPNs project to the PI and may release AstA in the morning to induce expression of *insulin-like peptide 3* and of the α-glucosidase *target of brain insulin* (*tobi*) as was shown by Hentze et al. (2015). Both are needed to metabolize food the flies have consumed during their feeding activity in the morning (Schäbler et al., 2020). Thus, the AstA release in the morning may regulate the flies' metabolic demands adapting them to a digestive energy-saving state during the siesta (Chen et al., 2016).

AstC shows a similar bimodal pattern in the LPNs as AstA, just with a lower peak in the morning. The E peak of AstC expression fits the crucial role of AstC in the timing of evening activity detected by Díaz et al. (2019)—under long or short photoperiods: a knock-down of AstC in all clock neurons led to a delay in the evening activity. Since AstC is not only expressed in the LPNs but additionally in several DN_{1p}s and DN_3s, it is not clear which of these clock neurons signal to the single LN_d that expresses the AstC receptor, but preliminary results show that all three types of neurons do so (Díaz et al., 2019). In addition, the LPNs could signal via AstC to the *insulin-like peptide 2* expressing neurons in the PI that express the AstC receptors Star1 and AICR2 and rhythmically inhibit reproduction (summarized in C. Zhang et al., 2021). C. Zhang et al. (2021) demonstrated a role of AstC signaling in female oogenesis rhythms via the AstC expressing DN_{1p}s. Rhythmic AstC release from the LPNs to the PI may contribute to this rhythm since the trough in LPN AstC coincides with the maximum of egg-laying in females that occurs in the late afternoon (Howlader & Sharma, 2006; Menon et al., 2014). The projection of an oviposition inhibitory neuron further supports the role of the LPNs in female reproduction.

DH31 in the LPNs is high throughout the day (showing only a weakly pronounced dip during the siesta) and rather low during the night, suggesting that it may be more important during the day than during the night. Indeed, DH31, which is a homolog of the vertebrate wake-promoting neuropeptide calcitonin, was shown to wake up the flies in the morning (Kunst et al., 2014). In addition, it is involved in the temperature preference of the flies, which is generally higher during the day than during the night (Goda et al., 2016). Both roles are thought to be mediated by certain DN_{1p}s, which express DH31 and the PDF receptor. PDF from the s-LN_vs activates these DN_{1p}s in the morning promoting DH31 secretion. Since DH31 can also activate the PDF receptor (Mertens et al., 2005), DH31 from the LPNs could additionally activate the DN_{1p}s and lead to DH31-mediated wakefulness not only in the morning but also in the evening. Similarly, DH31 in the evening

determines the temperature preference at night onset (Goda et al., 2016), and this may be supported by DH31 secretion from the LPNs.

4.4 | Ablation of the LPNs reveals their role in promoting morning and evening activity

As discussed above, the LPNs have multiple connections within the circadian clock network and beyond. Additionally, they express three neuropeptides with quite different and partially opposite functions. While AstA is sleep-promoting and controls feeding and metabolism, DH31 promotes wakefulness and AstC seems to modulate activity and perhaps egg-laying in the afternoon/evening. To test the prevailing function of the LPNs, we ablated them specifically with a cell-death gene and monitored activity and sleep in the LPN-less flies. This ablation did not affect the general rhythmicity of the flies but led to a lower power of the free-running rhythm, reduced activity in the morning and evening, and mildly increased sleep during the siesta and the second half of the night. The reduced morning and evening activity is in line with the wake-promoting role of DH31 during the day and coincides with the timing of the activity-promoting role of M and E neurons that are intimately connected with the LPNs. On the other hand, the slightly increased sleep during the siesta and the night appears to contradict the previously reported sleep-promoting role of LPN-derived AstA (Donlea et al., 2018; Ni et al., 2019) and the general strongly sleep-promoting role of the LPNs (Chen et al., 2016; Guo et al., 2018). There are several possible explanations for these discrepancies that we will discuss in the following.

Ni et al. (2019) used a newly generated AstA-lexA line to activate and silence the LPNs. This line drives expression in the LPNs and one prominent $AstA^{SP1}$ (SLP^{AstA}) neuron that projects into the dFB and appears to be predetermined for affecting sleep (see Donlea et al., 2018). Although the authors performed several additional manipulations indicating that the LPNs alone are sleep-promoting, it cannot be excluded that the $AstA^{SP1}$ neuron strongly contributes and completely overtakes the sleep-promotion after ablating the LPNs. Thus, the activity-promoting role of the LPNs may be the one that lacks after their ablation and consequently, the flies are less active and sleep more.

In the $AstA^{1}$- and $AstA^{34}$-Gal4 driver lines used by Chen et al. (2016), the $AstA^{SP1}$ neuron was not targeted. Instead, about four non-AstA positive neurons in the lateral cell body rind (LCBR cells) with unknown function were among the manipulated LPNs. These authors activated the LPNs and the unknown neurons with TrpA1 at 29°C and observed a highly increased sleep amount during the siesta and the night. The evening activity was almost completely suppressed, while morning activity was considerably reduced. Again, we cannot exclude that the unknown neurons are responsible for the observed increase in sleep, even though they do not project to any neuropils involved in sleep control (Chen et al., 2016). Nevertheless, when comparing the expression pattern and strength of $AstA^{1}$-/ $AstA^{34}$-Gal4 lines used by Chen et al. (2016) with those of our LPN-specific split-Gal4 line, another explanation appears more likely. While $AstA^{1}$-/$AstA^{34}$-Gal4 driven GFP was reliably and strongly present in two LPNs and only occasionally in all three LPNs, the GFP expression under the control of the LPN-specific split-Gal4 line was considerably weaker but usually present in all three LPNs. In this respect, it is interesting that the two LPNs targeted by Chen et al. (2016) lack the fibers running toward the anterior optic tubercle and look like the two similar LPNs that we describe in the present study (compare S1 movie in Chen et al., 2016 with Figure 6a). It is tempting to speculate that the two similar LPNs are the ones that promote sleep, while the third LPN with wider arborization patterns and different synaptic connections is activity-promoting.

If true, sleep should significantly increase when predominantly the two sleep-promoting LPNs are activated, while the moderate activation of all three LPNs should lead to complex changes, exactly as we have observed (moderate sleep increase during the day but not during the night and activity increase in the morning and evening). However, the ablation of all three LPNs should mainly reduce wakefulness during the morning and evening, because the wake-promoting LPN is now absent (and can perhaps be not replaced by other wake-promoting neurons), while other strongly sleep-promoting neurons are still present (e.g., the $AstA^{Sp1}$ neuron) that can easily overtake the sleep function. All this fits our observations.

Such heterogeneity within groups of clock neurons is not unusual and was, for example, described for the DN_{1p}s (Chatterjee et al., 2018; Guo et al., 2018; Lamaze et al., 2018). The study of Lamaze et al. (2018) is especially interesting in this respect because the authors found that the DN_{1p}s consist of sleep- and wakefulness-promoting neurons that can be distinguished by their morphology. The 6–9 sleep-promoting DN_{1p}s arborize in the PI and the posterior SMP and SLP (DN_{1p} neurons of type A), while the 5–6 wake-promoting DN_{1p}s form additionally a loop around the LH and project anteriorly toward the anterior optic tubercle (DN_{1p} neurons of type B). There, they inhibit sleep-promoting ring neurons of the ellipsoid body and thereby promote activity. Most interestingly, the unique putatively wake-promoting LPN forms a similar anteriorly projecting loop around the lateral horn (Figure 3c2) and might even be synaptically connected with the wake-promoting type B DN_{1p}s as suggested by one high confidence output synapse (Figure 7a2) and eight input synapses of middle to high confidence (Figure 7b2).

4.5 | Putative roles of the LPNs in the clock network and beyond

We summarize the putative connections and functions of the LPNs in a scheme (Figure 11). The LPNs get clock input from the M neurons (s-LN_vs) via PDF and possibly via regular synapses from the E neurons (LN_ds and 5th LN). They get input from a thermosensory neuron in the antennal glomeruli as well as from a female-specific oviposition inhibitory neuron. The LPNs signal via glutamate to two known central sleep centers, the dFB and the MBs, and additionally via AstA to the dFB. This results in a sleep-promoting function (Chen et al., 2016; Donlea et al., 2018; Ni et al., 2019; Figure 11b (ii)). Furthermore, the LPNs may signal via AstA to the PI, where they may contribute to the rhythmic control of metabolism and feeding (Chen et al., 2016; Hentze

et al., 2015). Via AstC and glutamate, the LPNs signal to the LN_ds and might impact evening activity (Díaz et al., 2019; Figure 11b (i)) and perhaps temperature entrainment, while their proposed AstC signaling to the PI may regulate rhythmic oviposition (C. Zhang et al., 2021). Via their third neuropeptide DH31, they might increase wakefulness by signaling to the PI (Kunst et al., 2014) and by interacting with the wake-promoting DN_{1p}s of type B (Lamaze et al., 2018) and additionally modulate temperature preference via the DN_2 (Goda et al., 2016; Figure 11b (iv)).

Regarding the broad arborization pattern of the LPNs in the SMP and SLP (Figure 11a), their heterogeneity, and their signaling to so far unknown neurons (e.g., the "U-shaped neurons"), we suppose further complex and modulatory roles of the LPNs, which have to be investigated in the future.

ACKNOWLEDGMENTS

This research was funded by the German Research Foundation (grants FO 207/16-1 and RI 2411/1-1) and the JSPS KAKENHI (19H03265). We thank Heinrich Dircksen for ITP antisera, Ralf Stanewsky for PER antisera and Takeshi Todo for CRY antisera, Jan Veenstra for antibodies against AstC, and DH31 as well as Hermann Steller for donating the UAS-hid line.

Open access funding enabled and organized by Projekt DEAL.

CONFLICT OF INTEREST

The authors declare no conflict of interest.

AUTHOR CONTRIBUTIONS

Nils Reinhard performed the experiments for the anatomical and connectivity studies, stainings, and analyzed time-dependent neuropeptide expression and parts of the behavioral experiments. Enrico Bertolini acquired data for the connectivity studies, Manabu Sekiguchi generated the LPN split-Gal4 line, and Aika Saito and Taishi Yoshii performed parts of the behavioral experiments. Nils Reinhard analyzed the data, compiled the figures, and wrote the first version of the manuscript. Charlotte Helfrich-Förster improved the manuscript and wrote the abstract and discussion with contributions from Nils Reinhard, Dirk Rieger, and Taishi Yoshii. Charlotte Helfrich-Förster, Dirk Rieger, and Taishi Yoshii conceived the project, supervised the study, and contributed to funding.

DATA AVAILABILITY STATEMENT

The data that support the findings of this study are available from the corresponding author upon reasonable request.

PEER REVIEW

The peer review history for this article is available at https://publons.com/publon/10.1002/cne.25294.

ORCID

Nils Reinhard https://orcid.org/0000-0002-7989-7150
Taishi Yoshii https://orcid.org/0000-0002-7057-7986
Dirk Rieger https://orcid.org/0000-0001-5597-5858
Charlotte Helfrich-Förster https://orcid.org/0000-0002-0859-9092

REFERENCES

Bates, A. S., Manton, J. D., Jagannathan, S. R., Costa, M., Schlegel, P., Rohlfing, T., & Jefferis, G. S. (2020). The natverse, a versatile toolbox for combining and analyzing neuroanatomical data. *eLife*, *9*, e53350. https://doi.org/10.7554/eLife.53350

Beckwith, E. J., & Ceriani, M. F. (2015). Communication between circadian clusters: The key to a plastic network. *Journal of Comparative Neurology*, *523*, 982–996. https://doi.org/10.1002/cne.23728

Bogovic, J. A., Otsuna, H., Heinrich, L., Ito, M., Jeter, J., Meissner, G., Nern, A., Colonell, J., Malkesman, O., Ito, K., & Saalfeld, S. (2020). An unbiased template of the *Drosophila* brain and ventral nerve cord. *Plos One*, *15*, e0236495. https://doi.org/10.1371/journal.pone.0236495

Buhmann, J., Sheridan, A., Malin-Mayor, C., Schlegel, P., Gerhard, S., Kazimiers, T., Krause, R., Nguyen, T. M., Heinrich, L., Lee, W.-C. A., Wilson, R., Saalfeld, S., Jefferis, G. S. X. E., Bock, D. D., Turaga, S. C., Cook, M., & Funke, J. (2021). Automatic detection of synaptic partners in a whole-brain *Drosophila* electron microscopy data set. *Nature Methods*, *18*, 771–774. https://doi.org/10.1038/s41592-021-01183-7

Chatterjee, A., Lamaze, A., De, J., Mena, W., Chélot, E., Martin, B., Hardin, P., Kadener, S., Emery, P., & Rouyer, F. (2018). Reconfiguration of a multi-oscillator network by light in the *Drosophila* circadian clock. *Current Biology*, *28*, 2007–2017.e4. https://doi.org/10.1016/j.cub.2018.04.064

Chen, J., Reiher, W., Hermann-Luibl, C., Sellami, A., Cognigni, P., Kondo, S., Helfrich-Förster, C., Veenstra, J. A., & Wegener, C. (2016). Allatostatin A signalling in *Drosophila* regulates feeding and sleep and is modulated by PDF. *Plos Genetics*, *12*, e1006346. https://doi.org/10.1371/journal.pgen.1006346

Cyran, S. A., Yiannoulos, G., Buchsbaum, A. M., Saez, L., Young, M. W., & Blau, J. (2005). The double-time protein kinase regulates the subcellular localization of the *Drosophila* clock protein period. *Journal of Neuroscience*, *25*, 5430–5437. https://doi.org/10.1523/JNEUROSCI.0263-05.2005

Díaz, M. M., Schlichting, M., Abruzzi, K. C., Long, X., & Rosbash, M. (2019). Allatostatin-C/AstC-R2 is a novel pathway to modulate the circadian activity pattern in *Drosophila*. *Current Biology*, *29*, 13–22.e3. https://doi.org/10.1016/j.cub.2018.11.005

Dircksen, H., Tesfai, L. K., Albus, C., & Nässel, D. R. (2008). Ion transport peptide splice forms in central and peripheral neurons throughout postembryogenesis of *Drosophila melanogaster*. *Journal of Comparative Neurology*, *509*, 23–41. https://doi.org/10.1002/cne.21715

Donlea, J. M., Pimentel, D., & Miesenböck, G. (2014). Neuronal machinery of sleep homeostasis in *Drosophila*. *Neuron*, *81*, 860–872. https://doi.org/10.1016/j.neuron.2013.12.013

Donlea, J. M., Pimentel, D., Talbot, C. B., Kempf, A., Omoto, J. J., Hartenstein, V., & Miesenböck, G. (2018). Recurrent circuitry for balancing sleep need and sleep. *Neuron*, *97*, 378–389.e4. https://doi.org/10.1016/j.neuron.2017.12.016

Dubruille, R., & Emery, P. (2008). A plastic clock: How circadian rhythms respond to environmental cues in *Drosophila*. *Molecular Neurobiology*, *38*, 129–145. https://doi.org/10.1007/s12035-008-8035-y

Duhart, J. M., Herrero, A., de la Cruz, G., Ispizua, J. I., Pírez, N., & Ceriani, M. F. (2020). Circadian structural plasticity drives remodeling of E cell output. *Current Biology*, *30*, 5040–5048.e5. https://doi.org/10.1016/j.cub.2020.09.057

Fujiwara, Y., Hermann-Luibl, C., Katsura, M., Sekiguchi, M., Ida, T., Helfrich-Förster, C., & Yoshii, T. (2018). The CCHamide1 neuropeptide expressed in the anterior dorsal neuron 1 conveys a circadian signal to the ventral lateral neurons in *Drosophila melanogaster*. *Frontiers Physiology*, *9*, 1276. https://doi.org/10.3389/fphys.2018.01276

Geissmann, Q., Rodriguez, L. G., Beckwith, E. J., & Gilestro, G. F. (2019). Rethomics: An R framework to analyze high-throughput behavioral data. *Plos One*, *14*, e0209331. https://doi.org/10.1371/journal.pone.0209331

Gentile, C., Sehadova, H., Simoni, A., Chen, C., & Stanewsky, R. (2013). Cryptochrome antagonizes synchronization of *Drosophila*'s circadian clock to temperature cycles. *Current Biology*, *23*, 185–195. https://doi.org/10.1016/j.cub.2012.12.023

Goda, T., Doi, M., Umezaki, Y., Murai, I., Shimatani, H., Chu, M. L., Nguyen, V. H., Okamura, H., & Hamada, F. N. (2018). Calcitonin receptors are ancient modulators for rhythms of preferential temperature in insects and body temperature in mammals. *Genes & Development*, *32*, 140–155. https://doi.org/10.1101/gad.307884.117

Goda, T., Tang, X., Umezaki, Y., Chu, M. L., & Hamada, F. N. (2016). *Drosophila* DH31 neuropeptide and PDF receptor regulate night-onset temperature preference. *J Neuroscience*, *36*, 11739–11754. https://doi.org/10.1523/JNEUROSCI.0964-16.2016

Guo, F., Holla, M., Díaz, M. M., & Rosbash, M. (2018). A circadian output circuit controls sleep-wake arousal in *Drosophila*. *Neuron*, *100*, 624–635.e4. https://doi.org/10.1016/j.neuron.2018.09.002

Guo, F., Yu, J., Jung, H. J., Abruzzi, K. C., Luo, W., Griffith, L. C., & Rosbash, M. (2016). Circadian neuron feedback controls the *Drosophila* sleep–activity profile. *Nature*, *536*, 292–297. https://doi.org/10.1038/nature19097

Hamada, F. N., Rosenzweig, M., Kang, K., Pulver, S. R., Ghezzi, A., Jegla, T. J., & Garrity, P. A. (2008). An internal thermal sensor controlling temperature preference in *Drosophila*. *Nature*, *454*, 217–220. https://doi.org/10.1038/nature07001

Helfrich-Förster, C. (1995). The period clock gene is expressed in central nervous system neurons which also produce a neuropeptide that reveals the projections of circadian pacemaker cells within the brain of *Drosophila melanogaster*. *Proceedings of the National Academy of Sciences of the United States of America*, *92*, 612–616. https://doi.org/10.1073/pnas.92.2.612

Helfrich-Förster, C., Shafer, O. T., Wülbeck, C., Grieshaber, E., Rieger, D., Taghert, P. (2007). Development and morphology of the clockgene-expressing lateral neurons of Drosophila melanogaster. *Journal of Comparative Neurology*, *500*, 47–70. https://doi.org/10.1002/cne.21146

Helfrich-Förster, C. (2014). From neurogenetic studies in the fly brain to a concept in circadian biology. *Journal of Neurogenetics*, *28*, 329–347. https://doi.org/10.3109/01677063.2014.905556

Helfrich-Förster, C. (2017). The drosophila clock system. In V. Kumar (Ed.) *Biological timekeeping: Clocks, rhythms, and behaviour* (pp. 133–176). Springer India. https://doi.org/10.1007/978-81-322-3688-7_6

Helfrich-Förster, C. (2018). Sleep in insects. *Annual Review of Entomology*, *63*, 69–86. https://doi.org/10.1146/annurev-ento-020117-043201

Hentze, J. L., Carlsson, M. A., Kondo, S., Nässel, D. R., & Rewitz, K. F. (2015). The neuropeptide allatostatin A regulates metabolism and feeding decisions in *Drosophila*. *Scientific Reports*, *5*, 11680. https://doi.org/10.1038/srep11680

Hergarden, A. C., Tayler, T. D., & Anderson, D. J. (2012). Allatostatin-A neurons inhibit feeding behavior in adult *Drosophila*. *Proceedings of the National Academy of Sciences of the United States of America*, *109*, 3967–3972. https://doi.org/10.1073/pnas.1200778109

Hermann-Luibl, C., Yoshii, T., Senthilan, P. R., Dircksen, H., & Helfrich-Förster, C. (2014). The ion transport peptide is a new functional clock neuropeptide in the fruit fly *Drosophila melanogaster*. *Journal of Neuroscience*, *34*, 9522–9536. https://doi.org/10.1523/JNEUROSCI.0111-14.2014

Herzog, E. D., Hermanstyne, T., Smyllie, N. J., & Hastings, M. H. (2017). Regulating the suprachiasmatic nucleus (SCN) circadian clockwork: Interplay between cell-autonomous and circuit-level mechanisms. *Cold Spring Harbor Perspectives in Biology*, *9*, a027706. https://doi.org/10.1101/cshperspect.a027706

Howlader, G., & Sharma, V. K. (2006). Circadian regulation of egg-laying behavior in fruit flies *Drosophila melanogaster*. *Journal of Insect Physiology*, *52*, 779–785. https://doi.org/10.1016/j.jinsphys.2006.05.001

Im, S. H., & Taghert, P. H. (2010). PDF receptor expression reveals direct interactions between circadian oscillators in *Drosophila*. *Journal of Comparative Neurology*, *518*, 1925–1945. https://doi.org/10.1002/cne.22311

Johnson, E. C., Shafer, O. T., Trigg, J. S., Park, J., Schooley, D. A., Dow, J. A., & Taghert, P. H. (2005). A novel diuretic hormone receptor in *Drosophila*: Evidence for conservation of CGRP signaling. *Journal of Experimental Biology*, *208*, 1239–1246. https://doi.org/10.1242/jeb.01529

Joiner, W. J., Crocker, A., White, B. H., & Sehgal, A. (2006). Sleep in *Drosophila* is regulated by adult mushroom bodies. *Nature*, *441*, 757. https://doi.org/10.1038/nature04811

Kaneko, M., & Hall, J. C. (2000). Neuroanatomy of cells expressing clock genes in *Drosophila*: Transgenic manipulation of the period and timeless genes to mark the perikarya of circadian pacemaker neurons and their projections. *Journal of Comparative Neurology*, *422*, 66–94. https://doi.org/10.1002/(SICI)1096-9861(20000619)422:1<66::AID-CNE5>3.0.CO;2-2

Kaneko, M., Helfrich-Förster, C., & Hall, J. C. (1997). Spatial and temporal expression of the period and timeless genes in the developing nervous system of *Drosophila*: Newly identified pacemaker candidates and novel features of clock gene product cycling. *Journal of Neuroscience*, *17*, 6745–6760. https://doi.org/10.1523/JNEUROSCI.17-17-06745.1997

King, A. N., & Sehgal, A. (2020). Molecular and circuit mechanisms mediating circadian clock output in the *Drosophila* brain. *European Journal of Neuroscience*, *51*, 268–281. https://doi.org/10.1111/ejn.14092

Klose, M., Duvall, L., Li, W., Liang, X., Ren, C., Steinbach, J. H., & Taghert, P. H. (2016). Functional PDF signaling in the *Drosophila* circadian neural circuit is gated by Ral A-dependent modulation. *Neuron*, *90*, 781–794. https://doi.org/10.1016/j.neuron.2016.04.002

Kunst, M., Hughes, M. E., Raccuglia, D., Felix, M., Li, M., Barnett, G., Duah, J., & Nitabach, M. N. (2014). Calcitonin gene-related peptide neurons mediate sleep-specific circadian output in *Drosophila*. *Current Biology*, *24*, 2652–2664. https://doi.org/10.1016/j.cub.2014.09.077

Lamaze, A., Krätschmer, P., Chen, K.-F., Lowe, S., & Jepson, J. E. C. (2018). A wake-promoting circadian output circuit in *Drosophila*. *Current Biology*, *28*, 3098–3105.e3. https://doi.org/10.1016/j.cub.2018.07.024

Liang, X., Holy, T. E., & Taghert, P. H. (2016). Synchronous *Drosophila* circadian pacemakers display nonsynchronous Ca^{2+} rhythms *in vivo*. *Science*, *351*, 976–981. https://doi.org/10.1126/science.aad3997

Liu, S., Liu, Q., Tabuchi, M., & Wu, M. N. (2016). Sleep drive is encoded by neural plastic changes in a dedicated circuit. *Cell*, *165*, 1347–1360. https://doi.org/10.1016/j.cell.2016.04.013

Majercak, J., Sidote, D., Hardin, P. E., & Edery, I. (1999). How a circadian clock adapts to seasonal decreases in temperature and day length. *Neuron*, *24*, 219–230. https://doi.org/10.1016/S0896-6273(00)80834-X

Menon, A., Varma, V., & Sharma, V. K. (2014). Rhythmic egg-laying behavior in virgin females of fruit flies *Drosophila melanogaster*. *Chronobiology International*, *31*, 433–441. https://doi.org/10.3109/07420528.2013.866131

Mertens, I., Vandingenen, A., Johnson, E. C., Shafer, O. T., Li, W., Trigg, J. S., De Loof, A., Schoofs, L., & Taghert, P. H. (2005). PDF receptor signaling in *Drosophila* contributes to both circadian and geotactic behaviors. *Neuron*, *48*, 213–219. https://doi.org/10.1016/j.neuron.2005.09.009

Michel, S., & Meijer, J. H. (2020). From clock to functional pacemaker. *European Journal of Neuroscience*, *51*, 482–493. https://doi.org/10.1111/ejn.14388

Mieda, M. (2020). The central circadian clock of the suprachiasmatic nucleus as an ensemble of multiple oscillatory neurons. *Neuroscience Research*, *156*, 24–31. https://doi.org/10.1016/j.neures.2019.08.003

Miyasako, Y., Umezaki, Y., & Tomioka, K. (2007). Separate sets of cerebral clock neurons are responsible for light and temperature entrainment of *Drosophila* circadian locomotor rhythms. *Journal of Biological Rhythms*, *22*, 115–126. https://doi.org/10.1177/0748730407299344

Ni, J. D., Gurav, A. S., Liu, W., Ogunmowo, T. H., Hackbart, H., Elsheikh, A., Verdegaal, A. A., & Montell, C. (2019). Differential regulation of the *Drosophila* sleep homeostat by circadian and arousal inputs. *eLife*, *8*, e40487. https://doi.org/10.7554/eLife.40487

Nicolai, L. J. J., Ramaekers, A., Raemaekers, T., Drozdzecki, A., Mauss, A. S., Yan, J., Landgraf, M., Annaert, W., & Hassan, B. A. (2010). Genetically encoded dendritic marker sheds light on neuronal connectivity in *Drosophila*. *Proceedings of the National Academy of Sciences of the*

United States of America, *107*, 20553–20558. https://doi.org/10.1073/pnas.1010198107

Park, D., Veenstra, J. A., Park, J. H., & Taghert, P. H. (2008). Mapping peptidergic cells in *Drosophila*: Where DIMM fits in. *Plos One*, *3*, e1896. https://doi.org/10.1371/journal.pone.0001896

Park, J. H., Helfrich-Förster, C., Lee, G., Liu, L., Rosbash, M., & Hall, J. C. (2000). Differential regulation of circadian pacemaker output by separate clock genes in *Drosophila*. *Proceedings of the National Academy of Sciences of the United States of America*, *97*, 3608–3613. https://doi.org/10.1073/pnas.070036197

Pfeiffer, B. D., Ngo, T.-T. B., Hibbard, K. L., Murphy, C., Jenett, A., Truman, J. W., & Rubin, G. M. (2010). Refinement of tools for targeted gene expression in *Drosophila*. *Genetics*, *186*, 735–755. https://doi.org/10.1534/genetics.110.119917

Pimentel, D., Donlea, J. M., Talbot, C. B., Song, S. M., Thurston, A. J. F., & Miesenböck, G. (2016). Operation of a homeostatic sleep switch. *Nature*, *536*, 333–337. https://doi.org/10.1038/nature19055

Pitman, J. L., McGill, J. J., Keegan, K. P., & Allada, R. (2006). A dynamic role for the mushroom bodies in promoting sleep in *Drosophila*. *Nature*, *441*, 753–756. https://doi.org/10.1038/nature04739

Pulver, S. R., Pashkovski, S. L., Hornstein, N. J., Garrity, P. A., & Griffith, L. C. 2009. Temporal dynamics of neuronal activation by channelrhodopsin-2 and TRPA1 determine behavioral output in *Drosophila* larvae. *Journal of Neurophysiology*, *101*, 3075–3088. https://doi.org/10.1152/jn.00071.2009

Rieger, D., Fraunholz, C., Popp, J., Bichler, D., Dittmann, R., & Helfrich-Förster, C. (2007). The fruit fly *Drosophila melanogaster* favors dim light and times its activity peaks to early dawn and late dusk. *Journal of Biological Rhythms*, *22*, 387–399. https://doi.org/10.1177/0748730407306198

Rieger, D., Shafer, O. T., Tomioka, K., & Helfrich-Förster, C. (2006). Functional analysis of circadian pacemaker neurons in *Drosophila melanogaster*. *Journal of Neuroscience*, *26*, 2531–2543. https://doi.org/10.1523/JNEUROSCI.1234-05.2006

Rieger, D., Stanewsky, R., & Helfrich-Förster, C. (2003). Cryptochrome, compound eyes, Hofbauer-Buchner eyelets, and ocelli play different roles in the entrainment and masking pathway of the locomotor activity rhythm in the fruit fly *Drosophila melanogaster*. *Journal of Biological Rhythms*, *18*, 377–391. https://doi.org/10.1177/0748730403256997

Rojas, P., Plath, J. A., Gestrich, J., Ananthasubramaniam, B., Garcia, M. E., Herzel, H., & Stengl, M. (2019). Beyond spikes: Multiscale computational analysis of in vivo long-term recordings in the cockroach circadian clock. *Network Neuroscience*, *3*, 944–968. https://doi.org/10.1162/netn_a_00106

Schäbler, S., Amatobi, K. M., Horn, M., Rieger, D., Helfrich-Förster, C., Mueller, M. J., Wegener, C., & Fekete, A. (2020). Loss of function in the *Drosophila* clock gene period results in altered intermediary lipid metabolism and increased susceptibility to starvation. *Cellular and Molecular Life Science*, *77*, 4939–4956. https://doi.org/10.1007/s00018-019-03441-6

Scheffer, L. K., Xu, C. S., Januszewski, M., Lu, Z., Takemura, S.-Y., Hayworth, K. J., Huang, G. B., Shinomiya, K., Maitlin-Shepard, J., Berg, S., Clements, J., Hubbard, P. M., Katz, W. T., Umayam, L., Zhao, T., Ackerman, D., Blakely, T., Bogovic, J., Dolafi, T., … Plaza, S. M.(2020). A connectome and analysis of the adult *Drosophila* central brain. *eLife*, *9*, e57443. https://doi.org/10.7554/eLife.57443

Schindelin, J., Arganda-Carreras, I., Frise, E., Kaynig, V., Longair, M., Pietzsch, T., Preibisch, S., Rueden, C., Saalfeld, S., Schmid, B., Tinevez, J.-Y., White, D. J., Hartenstein, V., Eliceiri, K., Tomancak, P., & Cardona, A. (2012). Fiji: An open-source platform for biological-image analysis. *Nature Methods*, *9*, 676–682. https://doi.org/10.1038/nmeth.2019

Schlichting, M., & Helfrich-Förster, C. (2015). Photic entrainment in *Drosophila* assessed by locomotor activity recordings. In A. Sehgal (Ed.), *Methods in enzymology. Vol. 552. Circadian rhythms and biological clocks, part B* (pp. 105–123) Academic Press. https://doi.org/10.1016/bs.mie.2014.10.017

Schlichting, M., Menegazzi, P., Rosbash, M., & Helfrich-Förster, C. (2019). A distinct visual pathway mediates high-intensity light adaptation of the circadian clock in *Drosophila*. *Journal of Neuroscience*, *39*, 1621–1630. https://doi.org/10.1523/JNEUROSCI.1497-18.2018

Schmid, B., Helfrich-Förster, & Yoshii, T. (2011). A new imageJ plug-in "ActogramJ" for chronobiological analyses. *Journal of Biological Rhythms*, *26*, 464–467. https://doi.org/10.1177/0748730411414264

Schubert, F. K., Hagedorn, N., Yoshii, T., Helfrich-Förster, C., & Rieger, D. (2018). Neuroanatomical details of the lateral neurons of *Drosophila melanogaster* support their functional role in the circadian system. *Journal of Comparative Neurology*, *526*, 1209–1231. https://doi.org/10.1002/cne.24406

Sekiguchi, M., Inoue, K., Yang, T., Luo, D.-G., & Yoshii, T. (2020). A catalog of GAL4 drivers for labeling and manipulating circadian clock neurons in *Drosophila melanogaster*. *Journal of Biological Rhythms*, *35*, 207–213. https://doi.org/10.1177/0748730419895154

Shafer, O. T., Helfrich-Förster, C., Renn, S. C. P., & Taghert, P. H. (2006). Reevaluation of *Drosophila melanogaster*'s neuronal circadian pacemakers reveals new neuronal classes. *Journal of Comparative Neurology*, *498*, 180–193. https://doi.org/10.1002/cne.21021

Stanewsky, R., Frisch, B., Brandes, C., Hamblen-Coyle, M. J., Rosbash, M., & Hall, J. C. (1997). Temporal and spatial expression patterns of transgenes containing increasing amounts of the *Drosophila* clock gene period and a lacZ reporter: Mapping elements of the PER protein involved in circadian cycling. *Journal of Neuroscience*, *17*, 676–696. https://doi.org/10.1523/JNEUROSCI.17-02-00676.1997

Stengl, M., & Arendt, A. (2016). Peptidergic circadian clock circuits in the Madeira cockroach. *Current Opinion in Neurobiology*, *41*, 44–52. https://doi.org/10.1016/j.conb.2016.07.010

Talay, M., Richman, E. B., Snell, N. J., Hartmann, G. G., Fisher, J. D., Sorkaç, A., Santoyo, J. F., Chou-Freed, C., Nair, N., Johnson, M., Szymanski, J. R., & Barnea, G. (2017). Transsynaptic mapping of second-order taste neurons in flies by trans-tango. *Neuron*, *96*, 783–795.e4. https://doi.org/10.1016/j.neuron.2017.10.011

Top, D., & Young, M. W. (2018). Coordination between differentially regulated circadian clocks generates rhythmic behavior. *Cold Spring Harbor Perspective in Biology*, *10*, a033589. https://doi.org/10.1101/cshperspect.a033589

Veenstra, J. A., Agricola, H.-J., & Sellami, A. (2008). Regulatory peptides in fruit fly midgut. *Cell and Tissue Research*, *334*:499–516. https://doi.org/10.1007/s00441-008-0708-3

Viswanath, V., Story, G. M., Peier, A. M., Petrus, M. J., Lee, V. M., Hwang, S. W., Patapoutian, A., & Jegla, T. (2003). Opposite thermosensor in fruitfly and mouse. *Nature*, *423*, 822–823. https://doi.org/10.1038/423822a

Vitzthum, H., Homberg, U., & Agricola, H. (1996). Distribution of Dip-allatostatin I-like immunoreactivity in the brain of the locust *Schistocerca gregaria* with detailed analysis of immunostaining in the central complex. *Journal of Comparative Neurology*, *369*, 419–437. https://doi.org/10.1002/(SICI)1096-9861(19960603)369:3<419::AID-CNE7>3.0.CO;2-8

Wagh, D. A., Rasse, T. M., Asan, E., Hofbauer, A., Schwenkert, I., Dürrbeck, H., Buchner, S., Dabauvalle, M.-C., Schmidt, M., Qin, G., Wichmann, C., Kittel, R., Sigrist, S. J., & Buchner, E. (2006). Bruchpilot, a protein with homology to ELKS/CAST, is required for structural integrity and function of synaptic active zones in *Drosophila*. *Neuron*, *49*, 833–844. https://doi.org/10.1016/j.neuron.2006.02.008

Wickham, H. (2016). *ggplot2: Elegant graphics for data analysis* (2nd ed.). Springer International Publishing. https://doi.org/10.1007/978-3-319-24277-4

Xie, X., Tabuchi, M., Corver, A., Duan, G., Wu, M. N., & Kolodkin, A. L. (2019). Semaphorin 2b regulates sleep-circuit formation in the *Drosophila* central brain. *Neuron*, *104*, 322–337.e14. https://doi.org/10.1016/j.neuron.2019.07.019

Yadlapalli, S., J.iang Chang, Bahle, A., Reddy, P., Meyhofer, E., & Shafer, O. T. (2018). Circadian clock neurons constantly monitor environmental temperature to set sleep timing. *Nature*, *555*, 98–102. https://doi.org/10.1038/nature25740

Yoon, J. G., & Stay, B. (1995). Immunocytochemical localization of *Diploptera punctata* allatostatin-like peptide in *Drosophila melanogaster*. *Journal of Comparative Neurology*, *363*, 475–488. https://doi.org/10.1002/cne.903630310

Yoshii, T., Heshiki, Y., Ibuki-Ishibashi, T., Matsumoto, A., Tanimura, T., & Tomioka, K. (2005). Temperature cycles drive *Drosophila* circadian oscillation in constant light that otherwise induces behavioral arrhythmicity. *European Journal of Neuroscience*, *22*, 1176–1184. https://doi.org/10.1111/j.1460-9568.2005.04295.x

Yoshii, T., Rieger, D., & Helfrich-Förster, C. (2012). Two clocks in the brain: An update of the morning and evening oscillator model in *Drosophila*. *Progress in Brain Research*, *199*, 59–82. https://doi.org/10.1016/B978-0-444-59427-3.00027-7

Yoshii, T., Todo, T., Wülbeck, C., Stanewsky, R., & Helfrich-Förster, C. (2008). Cryptochrome is present in the compound eyes and a subset of Drosophila's clock neurons. *Journal of Comparative Neurology*, *508*, 952–966. https://doi.org/10.1002/cne.21702

Yoshii, T., Vanin, S., Costa, R., Helfrich-Förster, C. (2009). Synergic Entrainment of Drosophila's Circadian Clock by Light and Temperature. *Journal of Biological Rhythms*, *24*, 452–464. https://doi.org/10.1177/0748730409348551

Yu, H.-H., Awasaki, T., Schroeder, M. D., Long, F., Yang, J. S., He, Y., Ding, P., Kao, J.-C., Wu, G. Y.-Y., Peng, H., Myers, G., & Lee, T. (2013). Clonal development and organization of the adult *Drosophila* central brain. *Current Biology*, *23*, 633–643. https://doi.org/10.1016/j.cub.2013.02.057

Zerr, D. M., Hall, J. C., Rosbash, M., & Siwicki, K. K. (1990). Circadian fluctuations of period protein immunoreactivity in the CNS and the visual system of *Drosophila*. *Journal of Neuroscience*, *10*, 2749–2762. https://doi.org/10.1016/j.cub.2013.02.057

Zhang, C., Daubnerova, I., Jang, Y.-H., Kondo, S., Žitňan, D., & Kim, Y.-J. (2021). The neuropeptide allatostatin C from clock-associated DN1p neurons generates the circadian rhythm for oogenesis. *Proceedings of the National Academy of Sciences of the United States of America*, *118*, e2016878118. https://doi.org/10.1073/pnas.2016878118

Zhang, Y. Q., Rodesch, C. K., & Broadie, K. (2002). Living synaptic vesicle marker: Synaptotagmin-GFP. *Genesis*, *34*, 142–145. https://doi.org/10.1002/gene.10144

Zhou, L., Schnitzler, A., Agapite, J., Schwartz, L. M., Steller, H., & Nambu, J. R. (1997). Cooperative functions of the reaper and head involution defective genes in the programmed cell death of *Drosophila* central nervous system midline cells. *Proceedings of the National Academy of Sciences of the United States of America*, *94*, 5131–5136. https://doi.org/10.1073/pnas.94.10.5131

How to cite this article: Reinhard, N., Bertolini, E., Saito, A., Sekiguchi, M., Yoshii, T., Rieger, D., & Helfrich-Förster, C. (2022). The lateral posterior clock neurons of *Drosophila melanogaster* express three neuropeptides and have multiple connections within the circadian clock network and beyond. *Journal of Comparative Neurology*, *530(9)*, 1507–1529. https://doi.org/10.1002/cne.25294